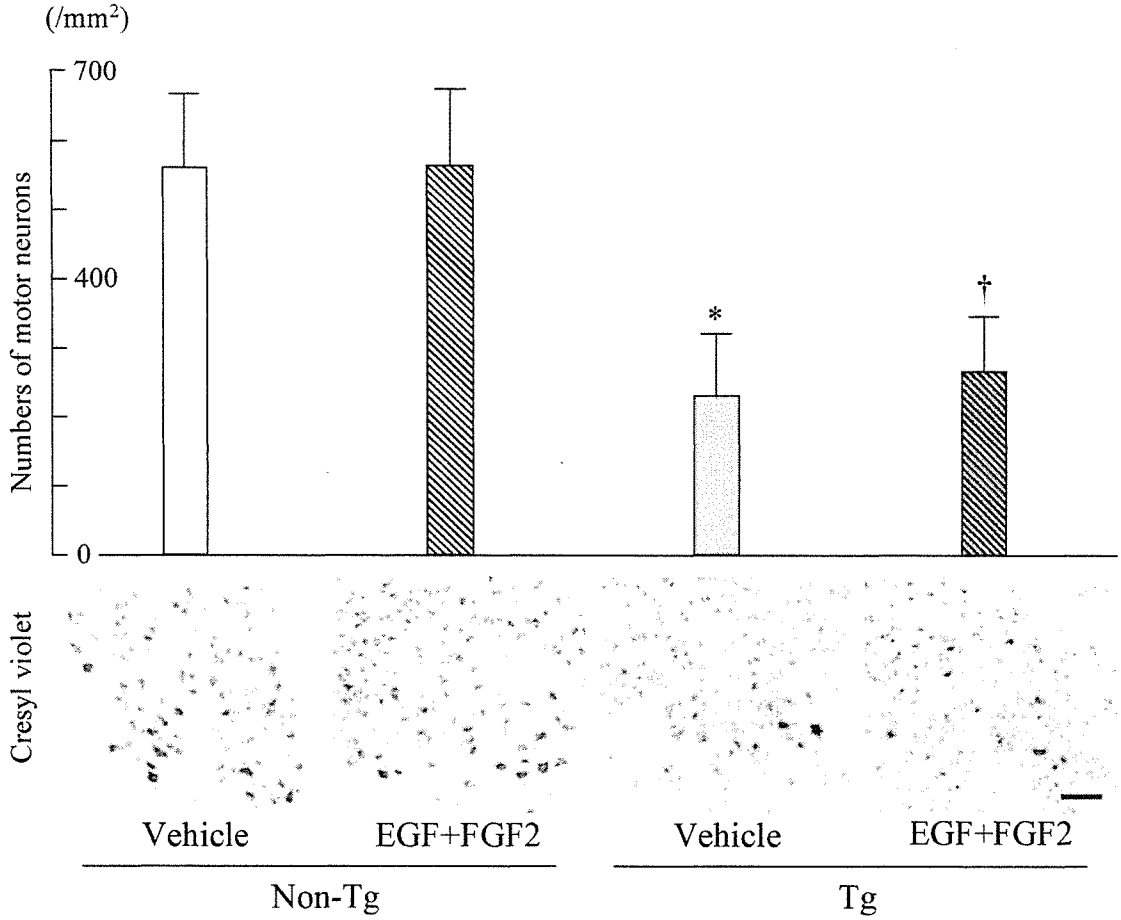

Fig. 2. Numbers (upper panel) and representative photomicrographs (lower panels) of motor neurons in the ventral horns (VH) of both non-Tg and Tg mice. Note the substantial motor neuron loss in Tg mice with or without EGF and FGF2 treatment compared with non-Tg mice (data are mean ± SD, $*P < 0.01$ vs. non-Tg mice treated with vehicle; $^{\dagger}P < 0.01$ vs. non-Tg mice treated with EGF and FGF2). Also note the similar numbers of motor neurons in Tg mice treated with vehicle and EGF and FGF2. Scale bar = 100 μm.

found to be larger than the number of BrdU + Iba1, BrdU + GFAP, and BrdU + PSA-NCAM double-labeled cells in the VH (Figs. 3, 4A,E,I,M, Table II) and in the DH (Figs. 3, 4B,F,J,N, Table II). Although the number of PSA-NCAM single-labeled cells and BrdU + PSA-NCAM double-labeled cells was smaller than the number of BrdU + nestin, BrdU + Iba1, or BrdU + GFAP double-labeled cells in the GM of both non-Tg and Tg mice, the increases in the rates of BrdU + PSA-NCAM double-labeled cells (3.2) were larger than those of BrdU + nestin (2.4), BrdU + Iba1 (1.2), or BrdU + GFAP (0.4) double-labeled cells in the GM of Tg mice with EGF and FGF2 treatment (Figs. 3, 4A,B,E,F,I,J,M,N, Table II). Although the number of nestin single-labeled cells increased less relative to Iba1 and GFAP in the GM, those in the WM increased more relative to Iba1 and GFAP in both non-Tg and Tg mice. Many BrdU-labeled cells expressed nestin and also (but to lesser extents) Iba1, GFAP, and PSA-NCAM in the WM of both non-Tg and Tg mice (Figs. 3, 4C,G,K,O, Table II). The number of nestin and PSA-NCAM single-labeled cells increased more relative to those labeled with Iba1 and GFAP in the CC of Tg mice, and the number of BrdU + nestin and BrdU + PSA-NCAM double-labeled cells was greater than the number of BrdU + Iba1 and BrdU + GFAP double-labeled cells (Figs. 3, 4D,H,L,P, Table II). Upon closer analysis of the GM, the number of BrdU + nestin double-labeled cells was found to be larger than the number of BrdU + Iba1, BrdU + GFAP, and BrdU + PSA-NCAM double-labeled cells only in the VH of Tg mice treated with EGF and FGF2, although the number of BrdU + Iba1 double-labeled cells was larger than the number of BrdU + nestin, BrdU + GFAP, and BrdU + PSA-NCAM double-labeled cells in both the VH and the DH of Tg mice treated with vehicle and non-Tg mice treated with vehicle and EGF and FGF2. (Figs. 3, 4A,B,E,F,I,J,M,N, Table II).

The total number of BrdU + nestin double-labeled cells in the vehicle-treated groups increased 3.7-fold in

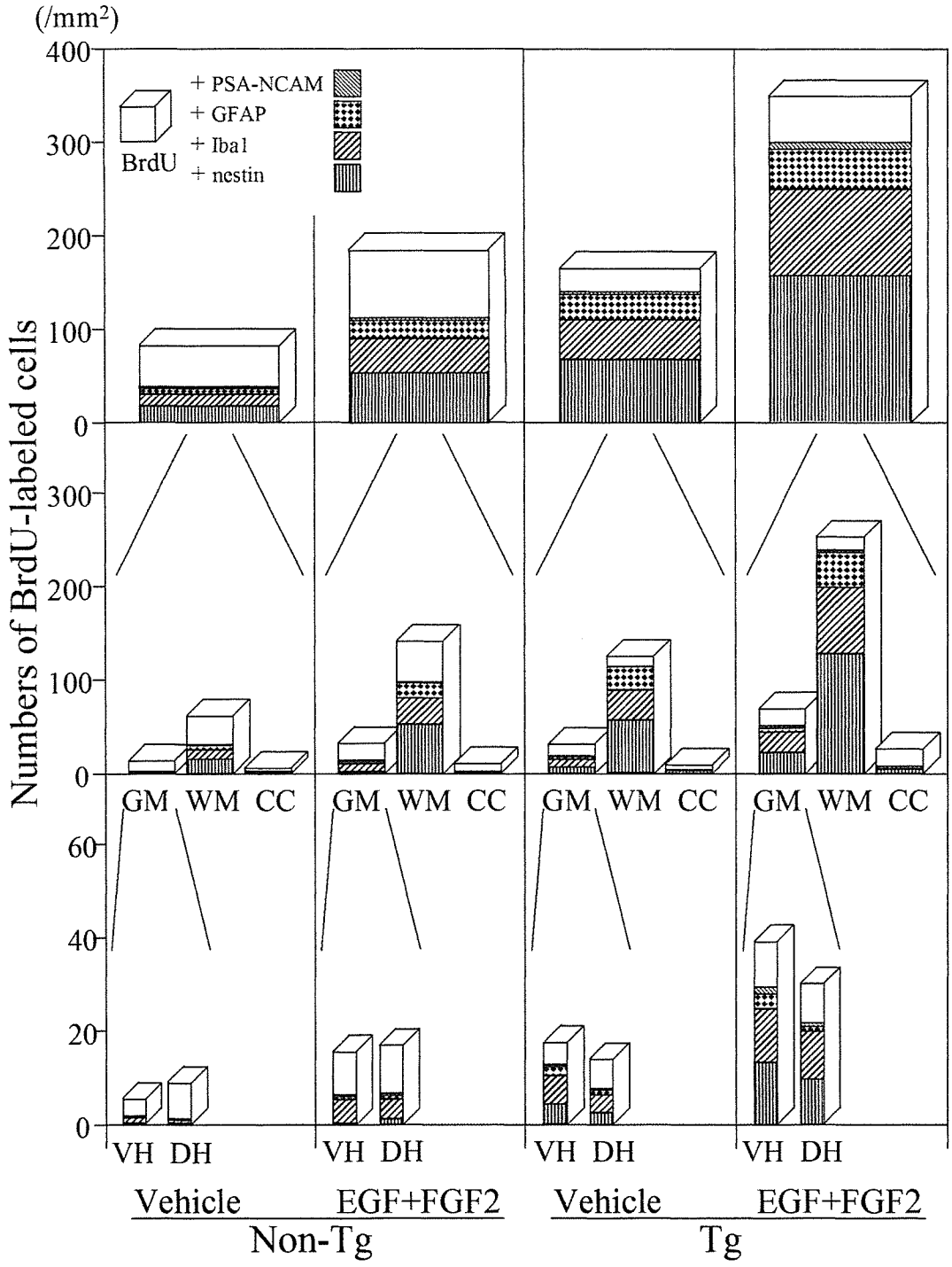

Fig. 3. Total numbers of BrdU-labeled cells and double-labeled cells with nestin, Iba1, GFAP, or PSA-NCAM in the lumbar spinal cords of all groups (top panels). Regional differences between the gray matter (GM), white matter (WM), and the ependyma of the central canal (CC; middle panels), and closer analysis of the VH and dorsal horns (DH) in the GM (bottom panels). Note that the total number of BrdU-labeled and BrdU + nestin double-labeled cells greatly increased in Tg mice treated with EGF and FGF2 (top panels). Upon regional analysis, the majority of BrdU-labeled and BrdU + nestin double-labeled cells were found to be located in the WM, with some in the GM and CC (middle panels). Closer analysis of the GM in vehicle-treated Tg mice revealed that the number of BrdU-labeled and BrdU + nestin double-labeled cells increased more in the VH than in the DH, which was greatly enhanced by treatment with EGF and FGF2 (bottom panels). See Results for details.

Tg mice (68.6 ± 49.7) compared with non-Tg mice (18.6 ± 14.2, $P < 0.01$; Fig. 3, Table II). Furthermore, the proportion of the total BrdU-labeled cells represented by the total BrdU + nestin double-labeled cells was larger in Tg mice (40.9%) than that in non-Tg mice (22.3%). Upon regional analysis, most BrdU + nestin double-labeled cells were found to be located in the WM, with some in the GM and CC in both non-Tg and Tg mice (Fig. 3, Table II). The proportion of BrdU-labeled cells represented by BrdU + nestin double-labeled cells was larger in the WM (non-Tg 27.1%; Tg 46.4%) than the GM in both non-Tg and Tg mice (non-Tg 3.5%; Tg 21.9%). The number of BrdU + nestin double-labeled cells and the proportion of those in the WM and GM of Tg mice (WM 46.4%; GM 21.9%) was larger than in non-Tg mice (WM 27.1%; GM

TABLE II. Numbers of BrdU-Labeled Cells and Double-Labeled Cells With Nestin, Ibal, GFAP, or PSA-NCAM in the Lumbar Spinal Cords†

Numbers of BrdU-labeled cells (/mm^2)	Non-Tg		Tg	
	Vehicle	EGF + FGF2	Vehicle	EGF + FGF2
BrdU				
Total	83.3 ± 31.8	187.9 ± 62.8*	167.7 ± 65.7*	354.6 ± 83.8**,***
Gray matter	14.4 ± 10.1	33.2 ± 16.5*	32.0 ± 15.8*	70.8 ± 25.0**,***
Ventral hom	5.5 ± 4.4	15.9 ± 9.2	17.7 ± 7.3****	39.9 ± 14.0*****
Dorsal hom	9.0 ± 6.5	17.4 ± 8.7	14.2 ± 9.3	30.9 ± 13.3
White matter	62.1 ± 27.3	143.0 ± 56.7*	126.2 ± 52.7*	256.7 ± 74.5**,***
Central canal	6.8 ± 5.9	11.7 ± 11.8	9.5 ± 7.4	27.2 ± 25.5**,***
BrdU + nestin				
Total	18.6 ± 14.2	54.7 ± 33.2	68.6 ± 49.7*	159.3 ± 89.2**
Gray matter	0.5 ± 0.8	1.3 ± 1.7	7.0 ± 6.7*	23.6 ± 15.2**
Ventral hom	0.1 ± 0.4	0.2 ± 0.5	4.4 ± 3.9	13.6 ± 9.9
Dorsal hom	0.3 ± 0.8	1.2 ± 1.4	2.5 ± 3.1	10.0 ± 6.1
White matter	16.8 ± 14.0	53.1 ± 32.9	58.5 ± 40.8*	130.4 ± 76.2**
Central canal	1.2 ± 3.1	0.2 ± 0.7	3.0 ± 5.5	5.3 ± 6.3
BrdU + Ibal				
Total	13.2 ± 14.1	38.2 ± 21.2	43.8 ± 26.2*	94.9 ± 55.3**
Gray matter	1.9 ± 2.4	9.5 ± 12.9	9.9 ± 10.8*	22.1 ± 19.0*
Ventral hom	1.2 ± 2.0	5.2 ± 8.0	6.1 ± 4.9	11.7 ± 10.1
Dorsal hom	0.6 ± 1.1	4.2 ± 4.9	3.9 ± 6.5	10.5 ± 11.3
White matter	11.3 ± 12.2	28.7 ± 16.0	33.8 ± 18.4*	72.7 ± 42.9**
Central canal	0.0 ± 0.0	0.0 ± 0.0	0.0 ± 0.0	0.0 ± 0.0
BrdU + GFAP				
Total	6.0 ± 5.5	19.0 ± 15.1	28.9 ± 17.8*	43.7 ± 17.9**
Gray matter	0.4 ± 0.6	1.5 ± 1.4	3.0 ± 3.4*	4.3 ± 5.6
Ventral hom	0.2 ± 0.5	0.6 ± 1.0	1.9 ± 2.8	3.4 ± 4.4
Dorsal hom	0.1 ± 0.5	0.9 ± 1.0	1.1 ± 1.4	1.0 ± 1.4
White matter	5.6 ± 5.6	17.1 ± 14.2	25.6 ± 15.8*	38.4 ± 14.8**
Central canal	0.0 ± 0.0	0.4 ± 1.4	0.3 ± 1.3	0.9 ± 2.7
BrdU + PSA-NCAM				
Total	2.1 ± 3.0	3.3 ± 2.7	3.1 ± 3.3	8.1 ± 7.1
Gray matter	0.0 ± 0.0	1.0 ± 1.5	0.6 ± 1.0	2.5 ± 3.7
Ventral hom	0.0 ± 0.0	0.4 ± 1.0	0.4 ± 0.9	1.6 ± 2.7
Dorsal hom	0.0 ± 0.0	0.6 ± 1.4	0.2 ± 0.6	0.8 ± 1.7
White matter	0.5 ± 0.5	0.7 ± 0.8	1.1 ± 1.3	2.9 ± 2.2**
Central canal	1.6 ± 2.6	1.6 ± 2.6	1.4 ± 2.4	2.7 ± 6.6

†After placement of the minipump, 50 mg/kg BrdU was intraperitoneally injected every 6 hr (four times per day) for 7 days, a total of 28 injections. At 121 days of age (21 days after minipump placement), total number; regional differences between the gray matter, white matter, and the ependyma of the central canal; and closer analysis of the ventral horns and dorsal horns in the gray matter of BrdU-labeled cells and double-labeled cells with nestin, Ibal, GFAP, or PSA-NCAM in the lumbar spinal cords (/mm^2) were evaluated. Data are presented as mean ± SD.

*$P < 0.01$ compared with non-Tg mice with vehicle.

**$P < 0.01$ compared with non-Tg mice with EGF and FGF2.

***$P < 0.01$ compared with Tg mice with vehicle.

****$P < 0.05$ compared with the posterior sides of Tg mice with vehicle.

*****$P < 0.01$ compared with the posterior sides of Tg mice with EGF and FGF2.

3.5%). Upon closer analysis of the GM in Tg mice, the number of BrdU + nestin double-labeled cells was found to be increased more in the VH (4.4 ± 3.9) than in the DH (2.5 ± 3.1; Fig. 3, Table II). The proportion of BrdU + nestin double-labeled cells in the VH (25.8%) was larger than that in the DH (17.6%).

With EGF and FGF2 treatment, the total number of BrdU + nestin double-labeled cells in both non-Tg and Tg mice (54.7 ± 33.2, 159.3 ± 89.2) increased 2.9- and 2.3-fold, respectively, compared with vehicle-treated mice (18.6 ± 14.2, 68.6 ± 49.7), and the total number of BrdU + nestin double-labeled cells in Tg mice (159.3 ± 89.2) was 2.9-fold that in non-Tg mice (54.7 ± 33.2, $P < 0.01$; Fig. 3, Table II). The proportion of total BrdU-labeled cells represented by total BrdU + nestin double-labeled cells was larger (non-Tg 29.1%; Tg 44.9%) in the EGF and FGF2 treated groups than in the vehicle-treated groups (non-Tg; 22.3%, Tg; 40.9%). Upon regional analysis, the number of BrdU + nestin double-labeled cells was found to be increased in the WM and GM relative to the vehicle

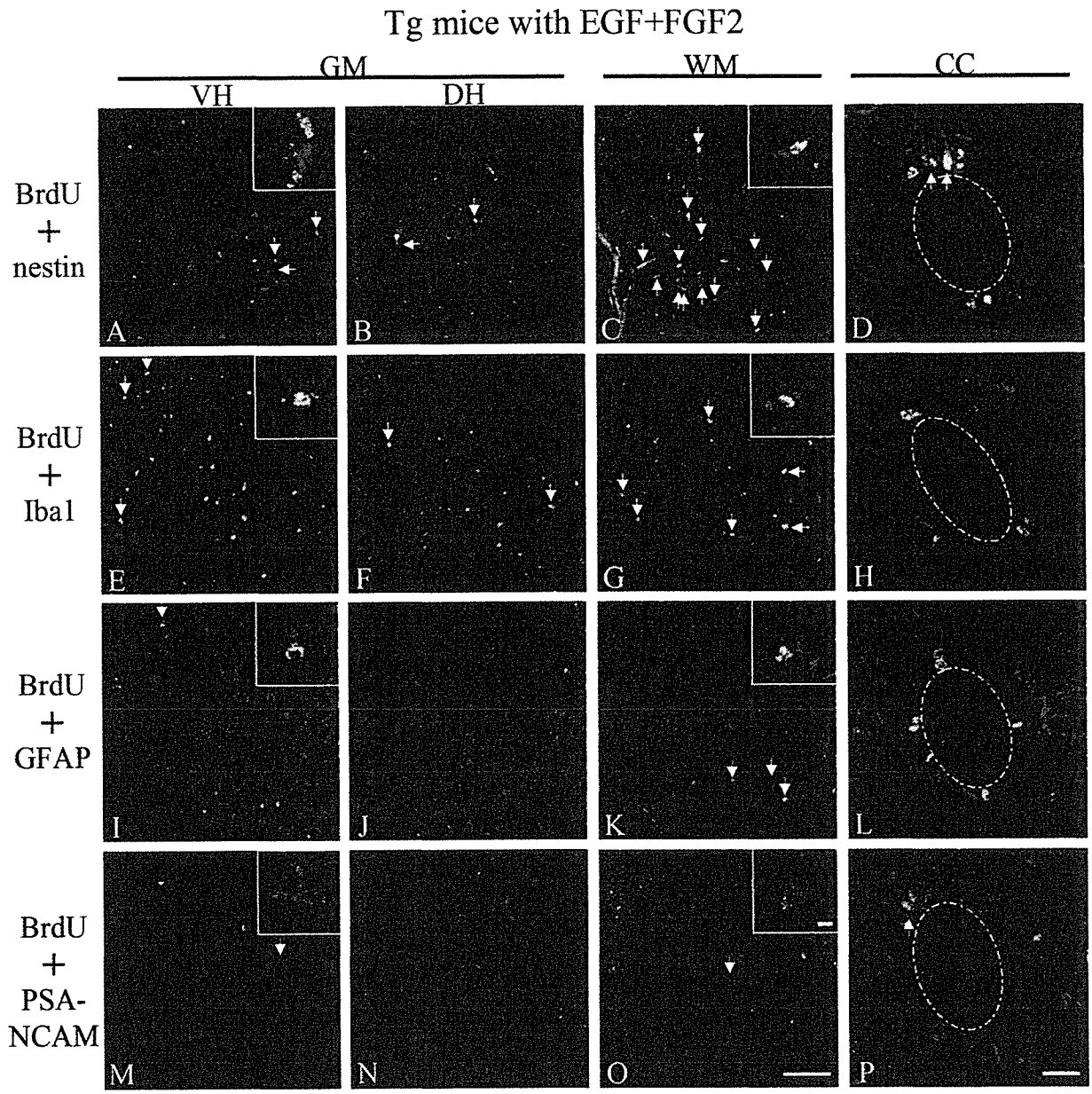

Fig. 4. Double-immunofluorescence analysis for BrdU (green) and nestin, Iba1, GFAP, PSA-NCAM (red) in Tg mice treated with EGF and FGF2. Many BrdU-labeled cells expressed nestin and also (to a lesser extent) Iba1, GFAP, and PSA-NCAM in the VH (**A,E,I,M,** arrows), DH (**B,F,** arrows; **J,N**), WM (**C,G,K,O,** arrows) and CC (**D,P,** arrows; **H,L**). Closer analysis of the GM showed that BrdU + nestin, Iba1, GFAP, and PSA-NCAM double-labeled cells increased more in the VH (A,E,I,M, arrows) than in the DH (B,F, arrows; J,N). The dashed circles in D,H,L,P indicate the central canal. Scale bars = 100 μm in O (applies to A–C,E–G,I–K,M–O); 10 μm in insets; 20 μm in P (applies to D,H,L,P).

in both non-Tg and Tg mice treated with EGF and FGF2, and that most nestin single-labeled and BrdU + nestin double-labeled cells were located in the WM, with some in the GM and CC (Figs. 3, 4A–D, Table II). However, the increase in the rate of BrdU + nestin double-labeled cells in the GM (2.4%) was larger than that in the WM (1.2%) and CC (0.8%) in Tg mice treated with EGF and FGF2. The proportion of BrdU-labeled cells in the WM and GM represented by the number of double-labeled cells in mice treated with EGF and FGF2 (non-Tg WM 37.1%; GM 3.9%; Tg WM 50.8%; GM 33.3%) was larger than that in the vehicle-treated mice (non-Tg WM 27.1%; GM 3.5%; Tg WM 46.4%; GM 21.9%). The same proportion in the WM and GM of Tg mice treated with EGF and FGF2 (WM; 50.8%, GM; 33.3%) was much larger than that in non-Tg mice treated with EGF and FGF2 (WM; 37.1%, GM; 3.9%). Upon closer analysis of the GM in both non-Tg and Tg mice treated with EGF and FGF2, the number

of BrdU + nestin double-labeled cells increased in both the VH and the DH compared with the vehicle-treated mice, and the number of nestin single-labeled and BrdU + nestin double-labeled cells increased more in the VH than in the DH in Tg mice (Figs. 3, 4A,B, Table II). In Tg mice, the proportion of BrdU-labeled cells represented by BrdU + nestin double-labeled cells in both VH and DH (VH 34.1%; DH 33.3%) was larger than that in vehicle-treated mice (VH 25.8%; DH 17.6%), and the number of those in the VH increased 3.1-fold compared with vehicle-treated mice.

The total number of BrdU + Iba1 double-labeled cells in the vehicle-treated groups increased 3.3-fold in Tg mice (43.8 ± 26.2) compared with the non-Tg mice (13.2 ± 14.1, $P < 0.01$; Fig. 3, Table II). Upon regional analysis, most BrdU + Iba1 double-labeled cells were found to be located in the WM, with some in the GM in both non-Tg and Tg mice (Fig. 3, Table II). Although the proportion of BrdU-labeled cells represented by BrdU + Iba1 double-labeled cells was larger in the WM (18.2%) than in the GM (13.2%) in non-Tg mice, the proportion was smaller in the WM (26.8%) than in the GM (30.9%) in Tg mice. Upon closer analysis of the GM in both non-Tg and Tg mice, the number of BrdU + Iba1 double-labeled cells were found to be increased more in the VH than in the DH (Fig. 3, Table II). With EGF and FGF2 treatment, the total number of BrdU + Iba1 double-labeled cells in both non-Tg and Tg mice increased 2.9- and 2.2-fold compared with that vehicle-treated mice (Fig. 3, Table II), respectively. Upon regional analysis, the numbers of BrdU + Iba1 double-labeled cells were found to be increased in the WM and GM in mice treated with EGF and FGF2 compared with vehicle-treated mice in both the non-Tg and the Tg groups, and most BrdU + Iba1 double-labeled cells were located in the WM, with some in the GM in both non-Tg and Tg mice, although the Iba1 single-labeled cells were located more in the GM, with some in the WM and CC in Tg mice (Figs. 3, 4E–H, Table II). Upon closer analysis of the GM in both non-Tg and Tg mice, the numbers of BrdU + Iba1 double-labeled cells were found to be increased in mice treated with EGF and FGF2 in both the VH and the DH compared with vehicle-treated mice, and the numbers of Iba1 single-labeled and BrdU + Iba1 double-labeled cells increased more in the VH than in the DH in Tg mice (Figs. 3, 4E,F, Table II).

The total number of BrdU + GFAP double-labeled cells in the vehicle-treated groups increased 4.8-fold in Tg mice (28.9 ± 17.8) compared with the non-Tg mice (6.0 ± 5.5, $P < 0.01$; Fig. 3, Table II). Upon regional analysis, most BrdU + GFAP double-labeled cells were found to be located in the WM, with some in the GM and CC in both non-Tg and Tg mice (Fig. 3, Table II). Upon closer analysis of the GM in both non-Tg and Tg mice, the number of BrdU + GFAP double-labeled cells was found to be increased more in the VH than in the DH (Fig. 3, Table II). With EGF and FGF2 treatment, the total number of BrdU + GFAP double-labeled cells in both non-Tg and Tg mice increased 3.2- and 1.5-fold compared with the vehicle-treated groups (Fig. 3, Table II), respectively. Upon regional analysis, the numbers of BrdU + GFAP double-labeled cells were found to be increased in the WM, GM, and CC in mice treated with EGF and FGF2 compared with the vehicle-treated groups for both non-Tg and Tg mice, and the majority of BrdU + GFAP double-labeled cells were located in the WM, with some in the GM and the CC in both non-Tg and Tg mice, although GFAP single-labeled cells were located mostly in the GM, with some in the WM and CC of Tg mice (Figs. 3, 4I–L, Table II). Upon closer analysis of the GM in Tg mice, the numbers of BrdU + GFAP double-labeled cells were found to be increased in the VH in mice treated with EGF and FGF2 compared with vehicle-treated mice, and the numbers of GFAP single-labeled and BrdU + GFAP double-labeled cells increased more in the VH than in the DH in Tg mice (Figs. 3, 4I,J, Table II).

The total number of BrdU + PSA-NCAM double-labeled cells in the vehicle-treated groups increased 1.5-fold in Tg mice (3.1 ± 3.3) compared with the non-Tg mice (2.1 ± 3.0; Fig. 3, Table II). Upon regional analysis, most BrdU + PSA-NCAM double-labeled cells were found to be located in the CC in both non-Tg and Tg mice (Figs. 3, 4E–H, Table II). Upon closer analysis of the GM in Tg mice, the numbers of BrdU + PSA-NCAM double-labeled cells were found to be increased more in the VH than in the DH (Fig. 3, Table II). With EGF and FGF2 treatment, the total number of BrdU + PSA-NCAM double-labeled cells in both non-Tg and Tg mice increased 2.5- and 1.5-fold compared with the vehicle-treated groups (Fig. 3, Table II), respectively. Upon regional analysis, the numbers of BrdU + PSA-NCAM double-labeled cells were found to be increased in the WM, GM, and CC in mice treated with EGF and FGF2 compared with the vehicle-treated groups for both non-Tg and Tg mice. The BrdU + PSA-NCAM double-labeled cells were located in the GM, WM, and CC equally in Tg mice, but the increase in the rate of BrdU + PSA-NCAM double-labeled cells in GM (3.2) was larger than that of WM (1.6) and CC (0.9), and PSA-NCAM single-labeled cells were located mostly in the GM and CC of Tg mice (Figs. 3, 4M–P, Table II). Upon closer analysis of the GM in Tg mice, the numbers of BrdU + PSA-NCAM double-labeled cells were found to be increased in both VH and DH in mice treated with EGF and FGF2 compared with vehicle-treated mice, and the number of PSA-NCAM single-labeled and BrdU + PSA-NCAM double-labeled cells increased more in the VH than in the DH in Tg mice (Figs. 3, 4M,N, Table II).

Triple-Immunofluorescence Analysis

Upon regional analysis, many nestin single-labeled cells expressed GFAP in the GM and WM of both non-Tg and Tg mice with or without EGF and FGF2 (Fig. 5A,B), but nestin single-labeled cells rarely expressed

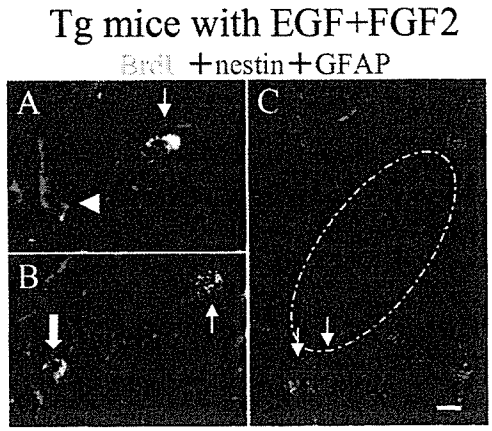

Fig. 5. Triple-immunofluorescence analysis for BrdU (green), nestin (red), and GFAP (blue) in Tg mice treated with EGF and FGF2. Many of the BrdU + nestin double-labeled cells did not express GFAP in the VH of GM (**A**; small arrow), WM (**B**; small arrow) and CC (**C**; small arrows), but many nestin single-labeled cells expressed GFAP in the GM (A; arrowhead) and WM, and some of the BrdU + nestin double-labeled cells expressed GFAP in the GM and WM (B; large arrow). The dashed circle indicates the central canal. Scale bar = 10 μm.

GFAP in the CC (Fig. 5C). The majority of BrdU + nestin double-labeled cells did not express GFAP in the CC of either non-Tg or Tg mice with or without EGF and FGF2 (Fig. 5C). In the GM and WM, many of the BrdU + nestin double-labeled cells did not express GFAP, but some of them expressed GFAP (Fig. 5A,B). In the case of BrdU + GFAP double-labeled cells, most of them expressed nestin in the GM, WM, and CC.

DISCUSSION

In the present study, we first observed that the number of BrdU + nestin double-labeled cells increased 3.7-fold in the spinal cords of Tg mice even without EGF and FGF2 treatment compared with non-Tg mice (Fig. 3, Table II). Treatment with EGF and FGF2 greatly increased the number of BrdU + nestin double-labeled cells in the spinal cords of both non-Tg and Tg mice (Fig. 3, Table II). With closer analysis of the GM of vehicle-treated groups, the number of BrdU + nestin double-labeled cells increased more in the VH than in the DH in Tg mice (Fig. 3, Table II), which was greatly enhanced by treatment with EGF and FGF2.

Among the vehicle-treated groups, the total number of BrdU-labeled cells increased 2.0-fold in the lumbar spinal cords of Tg mice compared with non-Tg mice at 21 days after minipump placement (Fig. 3, Table II), indicating that cell proliferation becomes active in Tg mice that have ALS. Double-labelling with BrdU + nestin, Iba1, GFAP, PSA-NCAM, or NeuN showed that many BrdU-labeled cells expressed nestin, and also Iba1, GFAP, and PSA-NCAM to a lesser extent, in both non-Tg and Tg mice but did not express NeuN. Although expression of nestin in the CNS is generally considered the marker of neural precursor cells (Reynolds and Weiss, 1992; Weiss et al., 1996; Gritti et al., 1996; Namiki and Tator, 1999; Schwartz et al., 2003; Chi et al., 2006), recent reports indicate that certain populations of adult neural precursor cells express GFAP (Doetsch et al., 1999; Rietze et al., 2001; Barres, 2003; Imura et al., 2003), and reactive astrocytes or immature astrocytes also express nestin in the injured spinal cord (Frisen et al., 1995; Lang et al., 2004). In the triple-immunofluorescence studies using BrdU, nestin, and GFAP, many BrdU + nestin-labeled cells did not express GFAP in the GM, WM, or CC, but some of them expressed GFAP in the GM and WM. The GFAP-negative BrdU + nestin double-labeled cells indicate the presence of real neural precurosor cells. However, BrdU + nestin + GFAP triple-labeled cells indicate the presence of astrocytogenesis or reactive astrocytosis, but some of them might be neural precursor cells too. As a result, we consider that most of the BrdU + nestin double-labeled cells are proliferating neural precursor cells. As previously determined for normal and pathological spinal cord (Horner et al., 2000; Strong et al., 2004; Zai and Wrathall, 2005; Chi et al., 2006), neural precursor cells proliferated more in Tg mice than in non-Tg mice and also proliferated more than microglial cells in both non-Tg and Tg mice. In an ischemic insult to the brain, the expression of the endogenous growth factors, such as EGF and FGF2, was significantly elevated (Naylor et al., 2005). In the spinal cords of mice with ALS, endogenous growth factors such as EGF and FGF2 might increase and neural precursor cells proliferate as a result.

Both EGF and FGF2 have neuroprotective effects against ischemic brain and spinal cord injury (Bethel et al., 1997; Kiprianova et al., 1999; Kojima and Tator, 2002), and they also have mitogenic effects on neural precursor cells in adult mouse or rat brain and spinal cord (Weiss et al., 1996; Kojima and Tator, 2002; Nakatomi et al., 2002; Martens et al., 2002). Although combination treatment with EGF and FGF2 may protect dying motor neurons in the spinal cords of mice with ALS, the present results indicate no such protective effect (Fig. 2, Table I). Neural regeneration can be divided into three steps: proliferation, migration, and differentiation (Gage, 2000; Iwai et al., 2002). Thus, we injected both EGF and FGF2 over only 7 days to stimulate neural precursor cell proliferation and sacrificed the mice 21 days after minipump placement to observe the migration and differentiation of the newly produced neural precursor cells during days 14–21. This treatment increased the numbers of BrdU + nestin, BrdU + PSA-NCAM, and BrdU + GFAP double-labeled cells relative to those in vehicle-treated mice, and the increase in the rate of BrdU + PSA-NCAM double-labeled cells was larger than that for BrdU + GFAP in GM of Tg mice (Fig. 3, Table II). Because the expression of PSA-NCAM in the CNS is generally considered a marker of neuronal precursor cells (Seki and Arai, 1993; Bonfanti and Theodosis, 1994; Rousselot et al., 1995; Doetsch and Alvarez-Buylla, 1996; Lois et al., 1996), we consider that the BrdU + PSA-NCAM double-labeled cells could

be proliferating neuronal precursor cells in the GM and CC. These results indicate that treatment with EGF and FGF2 potentiates the proliferation of neural precursor cells and their differentiation into neuronal precursor cells instead of astrocytes in GM of Tg mice.

A previous study showed that the majority of BrdU-labeled cells were located in the WM even at 1 hr after intraperitoneal BrdU injection in the normal spinal cord (Horner et al., 2000). Because neural precursor cells in the spinal cord reportedly reside close to the CC (Johansson et al., 1999; Martens et al., 2002), cells would be able to migrate from the CC to the WM rapidly. Nestin-labeled cells proliferate in the CC immediately after injury or after EGF and FGF2 treatment, and then the number in the CC is diminished because of migration to the WM and GM (Namiki and Tator, 1999; Kojima and Tator, 2002); astrocytes and oligodendrocytes increase slightly in the WM after injury or after EGF and FGF2 treatment (Martens et al., 2002; Zai and Wrathall, 2005). In the present study, most BrdU + nestin double-labeled cells were located in the WM, with some in the GM and CC, in all groups (Fig. 3, Table II). This suggests that most neural precursor cells that proliferated in the CC during BrdU labelling rapidly migrated to the WM, but few differentiated into astrocytes in the WM during the subsequent days 8–21. Although we did not extensively study oligodendrocytes, it appears that neural precursor cells seldom differentiated into oligodendrocytes in the WM.

Closer analysis of the GM showed that Tg itself increased the number of BrdU + nestin and BrdU + PSA-NCAM double-labeled cells, especially in the VH rather than the DH, which was greatly enhanced by treatment with EGF and FGF2 (Fig. 3, Table II). These results indicate that the migration of neural precursor cells to the VH with differentiation into neuronal precursor cells in VH is stimulated by motor neuron death associated with the SOD1 mutation and that EGF and FGF2 treatment enhances this migration of neural precursor cells to the GM and differentiation into neuronal precursor cells in the GM. In fact, treatment with EGF and FGF2 not only caused the proliferation of neural precursor cells but also potentiated their migration to the hippocampus and differentitaion into neuronal precursor cells and neurons after transient cerebral ischemia (Nakatomi et al., 2002).

The number of BrdU + nestin double-labeled cells was greater than the number of BrdU + GFAP double-labeled cells in the VH (Figs. 3, 4A,E,I, Table II) and DH (Figs. 3, 4B,F,J, Table II) of Tg mice, although the number of nestin single-labeled cells increased less than the number of GFAP single-labeled cells in the GM of Tg mice. Because most neural precursor cells remain immature rather than differentiating into astrocytes at 14–21 days after proliferation (Horner et al., 2000; Zai and Wrathall, 2005) and astrocytes start to increase in number in the GM, especially in the VH, during the presymptomatic stages of ALS (Hall et al., 1998; Yoshihara et al., 2002), most astrocytes observed at 21 days after minipump placement (Fig. 4I–L) were the cells that differentiated during the presymptomatic stages from neural precursor cells. Only small numbers of neural precursor cells differentiate into astrocytes during the symptomatic stages of ALS (Figs. 3, 4I–L, Table II), or they might have differentiated into astrocytes after 14 days (Kojima and Tator, 2002). Microglial cells are derived mainly from monocytes in pathological conditions (Kreutzberg, 1996), and they proliferate in the spinal cord during symptomatic ALS (Hall et al., 1998; Azari et al., 2005). Although some BrdU + Iba1 double-labeled cells might be BrdU-containing microglias resulting from phagocytosis, most of them will be labeled because of microglial proliferation. In the present study, microglial cells proliferated both in the WM and in the GM of Tg mice even with vehicle treatment (Fig. 3, Table II), and proliferation was enhanced both in non-Tg and in Tg mice with EGF and FGF2 treatment (Figs. 3, 4E–H, Table II).

In previous studies, neurogenesis was found in the subventricular zone of the lateral ventricle (Altman, 1969; Doetsch et al., 1997; Kornack and Rakic, 2001; Pencea et al., 2001) and the dentate gyrus of the hippocampus (Altman and Das, 1965; Kaplan and Hinds, 1977; Bayer et al., 1982; Cameron and McKay, 2001). Although extensive proliferation of intrinsic neural precursor cell activation and neurogenesis have been observed in the hippocampus after transient global ischemia with EGF and FGF2 treatment (Nakatomi et al., 2002), such activation has not been observed in pathological spinal cord even with EGF and FGF2 treatment (Gritti et al., 1996; Horner et al., 2000; Martens et al., 2002; Kojima and Tator, 2002; Mothe and Tator, 2005). Furthermore, in the present study, BrdU + NeuN double-labeled cells were not observed in Tg mice even with EGF and FGF2 treatment, although BrdU + PSA-NCAM double-labeled cells slightly increased in VH of Tg mice. However, the present study revealed extensive proliferation and migration of neural precursor cells to the VH, where they differentiate into neuronal precurosor cells with EGF and FGF2 treatment. Thus, the next step will be to induce the neural precursor cells to differentiate into motor neurons where they are dying because of ALS.

ACKNOWLEDGMENTS

This work was partially supported by Grants-in-Aid for Scientific Research (B) 15390273 and (Hoga) 15659338 and the National Project on Protein Structural and Functional Analyses from the Ministry of Education, Science, Culture and Sports of Japan and by grants from the Ministry of Health and Welfare of Japan (to Y. Itoyama, I. Kimura, and S. Kuzuhara).

REFERENCES

Abe K, Morita S, Kikuchi T, Itoyama Y. 1997. Protective effect of a novel free radical scavenger, OPC-14117, on Wobbler mouse motor neuron disease. J Neurosci Res 48:63–70.

Alonso G. 1999. Neuronal progenitor-like cells expressing polysialylated neural cell adhesion molecule are present on the ventricular surface of the adult rat brain and spinal cord. J Comp Neurol 414:149–166.

Altman J. 1969. Autoradiographic and histological studies of postnatal neurogenesis. J Comp Neurol 137:433–458.

Altman J, Das GD. 1965. Autoradiographic and histological evidence of postnatal hippocampal neurogenesis in rats. J Comp Neurol 124:319–335.

Alvarez-Buylla A, Garcia-Verdugo JM. 2002. Neurogenesis in adult subventricular zone. J Neurosci 22:629–634.

Azari MF, Profyris C, Le Grande MR, Lopes EC, Hirst J, Petratos S, Cheema SS. 2005. Effects of intraperitoneal injection of Rofecoxib in a mouse model of ALS. Eur J Neurol 12:357–364.

Barres BA. 2003. What is a glial cell? Glia 43:4–5.

Bayer SA, Yackel JW, Puri PS. 1982. Neurons in the rat dentate gyrus granular layer substantially increase during juvenile and adult life. Science 216:890–892.

Bethel A, Kirsch JR, Koehler RC, Finklestein SP, Traystman RJ. 1997. Intravenous basic fibroblast growth factor decreases brain injury resulting from focal ischemia in cats. Stroke 28:609–616.

Bonfanti L, Theodosis DT. 1994. Expression of polysialylated neural cell adhesion molecule by proliferating cells in the subependymal layer of the adult rat, in its rostral extension and in the olfactory bulb. Neuroscience 62:291–305.

Brown RH Jr, Robberecht W. 2001. Amyotrophic lateral sclerosis: pathogenesis. Semin Neurol 21:131–139.

Bruijn LI, Miller TM, Cleveland DW. 2004. Unraveling the mechanisms involved in motor neuron degeneration in ALS. Annu Rev Neurosci 27:723–749.

Cameron HA, McKay RD. 2001. Adult neurogenesis produces a large pool of new granule cells in the dentate gyrus. J Comp Neurol 435: 406–417.

Chi L, Ke Y, Luo C, Li B, Gozal D, Kalyanaraman B, Liu R. 2006. Motor neuron degeneration promotes neural progenitor cell proliferation, migration and neurogenesis in the spinal cords of ALS mice. Stem Cells 24:34–43.

Deng HX, Hentati A, Tainer JA, Iqbal Z, Cayabyab A, Hung WY, Getzoff ED, Hu P, Herzfeldt B, Roos RP, Warner C, Deng G, Soriano E, Smyth C, Parge HE, Ahmed A, Roses AD, Halliwell RA, Periak-Vance MA, Siddique T. 1993. Amyotrophic lateral sclerosis and structural defects in Cu/Zn superoxide dismutase. Science 261:1047–1051.

Doetsch F, Alvarez-Buylla A. 1996. Network of tangential pathways for neuronal migration in adult mammalian brain. Proc Natl Acad Sci U S A 93:14895–14900.

Doetsch F, Gracia-Verdugo JM, Alvarez-Buylla A. 1997. Cellular composition and three-dimensional organization of the subventricular germinal zone in the adult mammalian brain. J Neurosci 17:5046–5061.

Doetsch F, Caille I, Lim DA, Garcia-Verdugo JM, Alvarez-Buylla A. 1999. Subventricular zone astrocytes are neural stem cells in the adult mammalian brain. Cell 97:703–716.

Farah CA, Nguyen MD, Julien JP, Leclerc N. 2003. Altered levels and distribution of microtubule-associated proteins before disease onset in a mouse model of amyotrophic lateral sclerosis. J Neurochem 84:77–86.

Frisen J, Johansson CB, Torok C, Risling M, Lendahl U. 1995. Rapid, widespread, and longlasting induction of nestin contributes to the generation of glial scar tissue after CNS injury. J Cell Biol 131:453–464.

Gage FH. 2000. Mammalian neural stem cells. Science 287:1433–1438.

Ganel R, Ho T, Maragakis NJ, Jackson M, Steiner JP, Rothstein JD. 2006. Selective up-regulation of the glial Na^+-dependent glutamate transporter GLT1 by a neuroimmunophilin ligand results in neuroprotection. Neurobiol Dis 21:556–567.

Gritti A, Parati EA, Cova L, Frolichsthal P, Galli R, Wanke E, Faravelli L, Morassutti DJ, Roisen F, Nickel DD, Vescovi AL. 1996. Multipotential stem cells from the adult mouse brain proliferate and self-renew in response to basic fibroblast growth factor. J Neurosci 16:1091–1100.

Gurney ME, Pu H, Chiu AY, Canto MCD, Polchow CY, Alexander DD, Caliendo J, Hentati A, Kwon YW, Deng HX, Chen W, Zhai P, Sufit RL, Siddique T. 1994. Motor neuron degeneration in mice that express a human Cu/Zn superoxide dismutase mutation. Science 264:1772–1775.

Hall ED, Oostveen JA, Gurney ME. 1998. Relationship of microglial and astrocytic activation to disease onset and progression in a transgenic model of familial ALS. Glia 23:249–256.

Horner PJ, Power AE, Kempermann G, Kuhn HG, Palmer TD, Winkler J, Thal LJ, Gage FH. 2000. Proliferation and differentiation of progenitor cells throughout the intact adult rat spinal cord. J Neurosci 20: 2218–2228.

Imura T, Kornblum HI, Sofroniew MV. 2003. The predominant neural stem cell isolated from postnatal and adult forebrain but not early embryonic forebrain expresses GFAP. J Neurosci 23:2824–2832.

Iwai M, Sato K, Omori N, Nagano I, Manabe Y, Shoji M, Abe K. 2002. Three steps of neural stem cells development in gerbil dentate gyrus after transient ischemia. J Cereb Blood Flow Metab 22:411–419.

Iwai M, Sato K, Kamade H, Omori N, Nagano I, Shoji M, Abe K. 2003. Temporal profile of stem cell division, migration, and differentiation from subventricular zone to olfactory bulb after transient forebrain ischemia in gerbils. J Cereb Blood Flow Metab 23:331–341.

Jin K, Sun Y, Xie L, Peel A, Mao XO, Batteur S, Greenberg DA. 2003. Directed migration of neuronal precursors into the ischemic cerebral cortex and striatum. Mol Cell Neurosci 24:171–189.

Johansson CB, Momma S, Clarke DR, Risling M, Lendahl U, Frisen J. 1999. Identification of a neural stem cell in the adult mammalian central nervous system. Cell 96:25–34.

Kaplan MS, Hinds JW. 1977. Neurogenesis in the adult rat: electron microscopic analysis of light radioautographs. Science 197:1092–1094.

Kieran D, Hafezparast M, Bohnert S, Dick JR, Martin J, Schiavo G, Fisher EM, Greensmith L. 2005. A mutation in dynein rescues axonal transport defects and extends the life span of ALS mice. J Cell Biol 169:561–567.

Kiprianova I, Sandkühler J, Schwab S, Hoyer S, Spranger M. 1999. Brain-derived neurotrophic factor improves long-term potentiation and cognitive functions after transient forebrain ischemia in the rat. Exp Neurol 159:511–519.

Kirkinezos IG, Bacman SR, Hernandez D, Oca-Cossio J, Arias LJ, Perez-Pinzon MA, Bradley WG, Moraes CT. 2005. Cytochrome c association with the inner mitochondrial membrane is impaired in the CNS of G93A-SOD1 mice. J Neurosci 25:164–172.

Klivenyi P, Ferrante RJ, Matthews RT, Bogdanov MB, Klein AM, Andreassen OA, Mueller G, Wermer M, Kaddurah-Daouk R, Beal MF. 1999. Neuroprotective effects of creatine in a transgenic animal model of amyotrophic lateral sclerosis. Nat Med 5:347–350.

Kojima A, Tator CH. 2002. Intrathecal administration of epidermal growth factor and fibroblast growth factor 2 promotes ependymal proliferation and functional recovery after spinal cord injury in adult rats. J Neurotrauma 19:223–238.

Kornack DR, Rakic P. 2001. The generation, migration, and differentiation of olfactory neurons in the adult primate brain. Proc Natl Acad Sci U S A 96:4752–4757.

Kreutzberg GW. 1996. Microglia: a sensor for pathological events in the CNS. TIMS 19:312–318.

Lang B, Liu HL, Liu R, Feng GD, Jiao XY, Ju G. 2004. Astrocytes in injured adult rat spinal cord may acquire the potential of neural stem cells. Neuroscience 128:775–783.

Lois C, Garcia-Verdugo JM, Alvarez-Buylla A. 1996. Chain migration of neuronal precursors. Science 271:978–981.

Manabe Y, Nagano I, Gazi MS, Murakami T, Shiote M, Shoji M, Kitagawa H, Setoguchi Y, Abe K. 2002. Adenovirus-mediated gene transfer of glial cell line-derived neurotrophic factor prevents motor neuron loss of transgenic model mice for amyotrophic lateral sclerosis. Apoptosis 7:329–334.

Manfredi G, Xu Z. 2005. Mitochondrial dysfunction and its role in motor neuron degeneration in ALS. Mitochondrion 5:77–87.

Martens DJ, Seaberg RM, van der Kooy D. 2002. In vivo infusions of exogenous growth factors into the fourth ventricle of the adult mouse brain increase the proliferation of nerural progenitors around the fourth ventricle and the central canal of the spinal cord. Eur J Neurosci 16:1045–1057.

Menzies FM, Ince PG, Shaw PJ. 2002. Mitochondrial involvement in amyotrophic lateral sclerosis. Neurochem Int 40:543–551.

Mothe AJ, Tator CH. 2005. Proliferation, migration, and differentiation of endogenous ependymal region stem/progenitor cells following minimal spinal cord injury in the adult rat. Neuroscience 131:177–187.

Murakami T, Ilieva H, Shiote M, Nagata T, Nagano I, Shoji M, Abe K. 2003. Hypoxic induction of vascular endothelial growth factor is selectively impaired in mice carrying the mutant SOD1 gene. Brain Res 989:231–237.

Nakatomi H, Kuriu T, Okabe S, Yamamoto S, Hatano O, Kawahara N, Tamura A, Kirino T, Nakafuku M. 2002. Regeneration of hippocampal pyramidal neurons after ischemic brain injury by recruitment of endogenous neural progenitors. Cell 110:429–441.

Namiki J, Tator CH. 1999. Cell proliferation and nestin expression in the ependyma of the adult rat spinal cord after injury. J Neuropathol Exp Neurol 58:489–498.

Narai H, Nagano I, Ilieva H, Shiote M, Nagata T, Hayashi T, Shoji M, Abe K. 2005. Prevention of spinal motor neuron death by insulin-like growth factor-1 associating with the signal transduction systems in SODG93A transgenic mice. J Neurosci Res 82:452–457.

Naylor M, Bowen KK, Sailor KA, Dempsey RJ, Vemuganti R. 2005. Preconditioning-induced ischemic tolerance stimulates growth factor expression and neurogenesis in adult rat hippocampus. Neurochem Int 47:565–572.

Pencea V, Bingaman KD, Freedman LJ, Luskin MB. 2001. Neurogenesis in the subventricular zone and rostral migratory stream of the neonatal and adult primate forebrain. Exp Neurol 172:1–16.

Rao MV, Nixon RA. 2003. Defective neurofilament transport in mouse models of amyotrophic lateral sclerosis: a review. Neurochem Res 28: 1041–1047.

Reynolds BA, Weiss S. 1992. Generation of neurons and astrocytes from isolated cells of the adult mammalian central nervous system. Science 255:1707–1710.

Rice AC, Khaldi A, Harvey HB, Salman NJ, White F, Fillmore H, Bullock MR. 2003. Proliferation and neuronal differentiation of mitotically active cells following traumatic brain injury. Exp Neurol 183:406–417.

Rietze RL, Valcanis H, Brooker GF, Thomas T, Voss AK, Bartlett PF. 2001. Purification of a pluripotent neural stem cell from the adult mouse brain. Nature 412:736–739.

Rosen DR, Siddique T, Patterson D, Figlewich DA, Sapp P, Hentati A, Donaldson D, Goto J, O'Regan JP, Deng HXRahmani Z, Krizus A, Mckenna-Yasek D, Cayabyab A, Gaston SM, Berger R, Tanzi RE, Halperin JJ, Herzfeldt B, Bergh RVD, Hung WY, Bird T, Deng G, Mulder DW, Smyth C, Laing NG, Soriano E, Pericak-Vance MA, Haines J, Rouleau GA, Gusella JS, Horvitz HR, Brown RH. 1993. Mutations in Cu/Zn superoxide dismutase gene are associated with familial amyotrophic lateral sclerosis. Nature 362:59–62.

Rousselot P, Lois C, Alvarez-Buylla A. 1995. Embryonic (PSA) N-CAM reveals chains of migrating neuroblasts between the lateral ventricle and the olfactory bulb of adult mice. J Comp Neurol 35:51–61.

Schwartz PH, Bryant PJ, Fuja TJ, Su H, O'Dowd DK, Klassen H. 2003. Isolation and characterization of neural progenitor cells from post-mortem human cortex. J Neurosci Res 74:838–851.

Seki T, Arai Y. 1993. Distribution and possible roles of the highly polysialylated neural cell adhesion molecule (NCAM-H) in the developing and adult central nervous system. Neurosci Res 17:265–290.

Strong MJ, Leystra-Lantz C, Ge WW. 2004. Intermediate filament steady-state mRNA levels in amyotrophic lateral sclerosis. Biochem Biophys Res Commun 316:317–322.

Weiss S, Dunne C, Hewson J, Wohl C, Wheatley M, Peterson AC, Reynolds BA. 1996. Multipotent CNS stem cells are present in the adult mammalian spinal cord and ventricular neuroaxis. J Neurosci 16: 7599–7609.

Wong PC, Pardo CA, Borchelt DR, Lee MK, Copeland NG, Jenkins NA, Sisodia SS, Cleveland DW, Price DL. 1995. An adverse property of a familial ALS-linked SOD1 mutation causes motor neuron disease characterized by vacuolar degeneration of mitochondrial. Neuron 14:1105–1116.

Yagita Y, Kitagawa K, Ohtsuki T, Takasawa Ki, Miyata T, Okano H, Hori M, Matsumoto M. 2001. Neurogenesis by progenitor cells in the ischemic adult rat hippocampus. Stroke 32:1890–1896.

Yoshihara T, Ishigaki S, Yamamoto M, Liang Y, Niwa J, Takeuchi H, Doyu M, Sobue G. 2002. Differential expression of inflammation- and apoptosis-related genes in spinal cords of a mutant SOD1 transgenic mouse model of familial amyotrophic lateral sclerosis. J Neurochem 80: 158–167.

Zai LJ, Wrathall JR. 2005. Cell proliferation and replacement following contusive spinal cord injury. Glia 50:247–257.

Histol Histopathol (2006) 21: 729-742

http://www.hh.um.es

Histology and Histopathology
Cellular and Molecular Biology

Histological recovery of the hepatocytes is based on the redox system upregulation in the animal models of mutant superoxide dismutase (SOD)1-linked amyotrophic lateral sclerosis

M. Kato[1], S. Kato[2], Y. Abe[3], T. Nishino[3], E. Ohama[2], M. Aoki[4] and Y. Itoyama[4]

[1]Division of Pathology, Tottori University Hospital, [2]Department of Neuropathology, Institute of Neurological Sciences, Faculty of Medicine, Tottori University, Yonago, Japan, [3]Department of Biochemistry and Molecular Biology, Nippon Medical School, Tokyo and [4]Department of Neuroscience, Division of Neurology, Tohoku University Graduate School of Medicine, Sendai, Japan

Summary. Histological rescue of superoxide dismutase1 (SOD1)-mutated hepatocytes from mutant SOD1 stress is investigated from the viewpoint of upregulation of the redox system [peroxiredoxin (Prx) and glutathione peroxidase (GPx)]. Histopathological and immunohistochemical studies using antibodies against PrxI/PrxII/GPxI were carried out on specimens from four different strains of animal models of mutant SOD1-linked familial amyotrophic lateral sclerosis (ALS). In the livers of the ALS animal models in the presymptomatic stage without motor neuron loss, both swollen and eosinophilic hepatocytes with vacuolation pathology were observed. After developing motor deficits, this swelling and vacuolation ceased to be apparent. In the terminal stage when severe motor neuron loss was observed, these hepatocytes recovered and appeared normal. In redox system-related immunohistochemical preparations, almost all of the normal hepatocytes expressed the redox system-related enzymes PrxI/PrxII/GPxI. In the presymptomatic stage, some hepatocytes did not express redox system-related enzymes. After clinical onset, over 75% of hepatocytes showed overexpression of PrxI/PrxII/GPxI, i. e., upregulation of the redox system. At the end stage, near normal PrxI/PrxII/GPxI expression was observed again in the hepatocytes. Redox system upregulation in SOD1-mutated hepatocytes rescues hepatocytes from the mutant SOD1 stress that leads to motor neuron death.

Offprint requests to: Masako Kato, M.D., Ph.D., Division of Pathology, Tottori University Hospital, Nishi-cho 36-1, Yonago 683-8504, Japan. e-mail: makato@grape.med.tottori-u.ac.jp, Shinsuke Kato, M.D., Ph.D., Department of Neuropathology, Institute of Neurological Sciences, Faculty of Medicine, Tottori University, Nishi-cho 36-1, Yonago 683-8504, Japan. e-mail: kato@grape.med.tottori-u.ac.jp

Key words: Amyotrophic lateral sclerosis, Hepatocyte, Redox system, Peroxiredoxin, Superoxide dismutase1

Introduction

In general, living cells under aerobic conditions produce reactive oxygen species (ROSs) during physiological processes and in response to external stimuli such as ultraviolet radiation and chemical agents. In order to protect themselves from potentially destructive ROSs, cells have developed antioxidant enzyme defense systems. In these systems, there are two groups of enzymes; the enzymes of the first group convert superoxide radicals to hydrogen peroxide (H_2O_2), and the enzymes of the second group convert H_2O_2 to harmless water (H_2O) and oxygen (O_2). In the first group, three isoforms of superoxide dismutase (SOD) [EC 1.15.1.1] have been identified: SOD1, SOD2, and SOD3 (Fridovich, 1986; Abe and Okazaki, 1987), and in the second group, there are the peroxiredoxin-(Prx-) and glutathione peroxidase-(GPx-) families, as well as catalase that is localized in peroxisomes. The enzymes of the Prx- and GPx-families are considered to be important players that directly control the redox system.

The Prx-families have been identified in a large number of organisms (Chae et al., 1993, 1994; Prosperi et al., 1993; Hirotsu et al., 1999b; Hofmann et al., 2002). PeroxiredoxinI (PrxI) is an intracellular antioxidant protein that is expressed preferentially in the liver (Iwahara et al., 1995). PeroxiredoxinII (PrxII) is also a novel organ-specific antioxidative enzyme that is expressed in the mammalian central nervous system (Matsumoto et al., 1999; Kato et al., 2004) as well as the liver. The GPx-family is composed of at least four GPx

isoforms in mammals (de Haan et al., 1998), and GPxI is thought to be the major enzyme responsible for removing intracytoplasmic H_2O_2. Furthermore, the redox system regulates various control mechanisms in signal transduction and gene expression (Sen and Packer, 1996). This redox signal transduction is linked to important biological systems such as apoptosis, cellular differentiation, immune response and growth control (Jin et al., 1997; Wen and Van etten, 1997).

Amyotrophic lateral sclerosis (ALS) is a fatal neurodegenerative disorder that selectively involves both upper and lower motor neurons (Kato et al., 2003). The prevalence rate of ALS is approximately 5 to 10 cases per 100,000 population (de Belleroche et al., 1996). Five to ten per cent of ALS cases are familial, although most ALS cases are sporadic (Hudson, 1981; Juneja et al., 1997). The disease has been studied for over 130 years since Charcot and Joffroy (1869) first reported it in 1869. In 1991, linkage analysis of certain familial ALS (FALS) patients demonstrated that the genetic locus is strongly linked to chromosome 21q (Siddique et al., 1991). Deng et al. (1993) and Rosen et al. (1993) indicated in 1993 that this locus partially overlaps the genetic locus of SOD1 on chromosome 21. Based on this discovery, human mutated SOD1-expressing transgenic mice have been developed and human mutated-SOD1 causes progressive motor neuron degeneration and death with a similar course to that in human ALS (Gurney et al., 1994). Nagai et al. have successfully produced two types of transgenic rat expressing human SOD1 with H46R and G93A mutations (Nagai et al., 2001). Pathologically, mutant SOD1 causes motor neuron death in the in vivo milieu where it exists, that is, in familial ALS patients with SOD1 gene mutation and transgenic animals expressing human mutant SOD1 (Kato et al., 2003). The exact mechanism of the motor neuron death based on mutant SOD1 is still unclear although there are many hypotheses, including copper toxicity, hydroxy radical toxicity, peroxynitrite toxicity, and aggregation toxicity (Kato et al., 1999, 2000, 2003). In addition, ALS is a heterogeneous disease including sporadic ALS of unknown etiology, familial ALS with SOD1 gene mutation and transgenic animal models with human mutant SOD1. Despite the heterogeneous pathogenesis of ALS, its essential neuropathology is motor neuron death. In the spinal cord, the common, consistent neuropathological finding among sporadic ALS of unknown etiology, familial ALS with SOD1 gene mutation and transgenic animal models with human mutant SOD1 is loss of the anterior horn cells (Kato et al., 1999, 2000, 2003). Because SOD1 is most abundant in the liver (Westman and Marklund, 1981; Iwahara et al., 1995), and mutant SOD1 is concentrated in the liver milieu where mutant SOD1 exists, the toxicity of mutant SOD1 should be most evident in the liver. Anterior horn cells of the spinal cord and hepatocytes are equally involved in mutant SOD1 stress. However, the essential pathological feature of SOD1-mutated FALS patients and human mutant SOD1-linked ALS model animals is cell death in anterior horn cells but not in hepatocytes. In other words, although anterior horn cells and hepatocytes are under the same mutant SOD1 stress, cell death is observed histopathologically only in the anterior horn cells. Given that the redox system-related proteins PrxI, PrxII and GPxI (PrxI/PrxII/GPxI) that are directly linked to SOD1 (mutant SOD1) are also most abundant in hepatocytes (Westman and Marklund., 1981; Iwahara et al., 1995), we sought to elucidate immunohistochemically the mechanism by which SOD1-mutated hepatocytes survive while SOD1-mutated anterior horn cells die.

Materials and methods

Animal models

Histochemical and immunohistochemical studies were carried out on specimens from ALS animal models: transgenic mice and rats carrying the overexpressed human mutant SOD1 genes. The G93A mice used in this study were two types of transgenic mice carrying the overexpressed human G93A mutant SOD1 gene: high copy G93A mice (G1H, B6SJL-TgN[SOD1-G93A]1Gur; 20-30 copies of the transgene) (G1H-G93A mice) and low copy G93A mice (G1L, B6SJL-TgN[SOD1-G93A]1Gur^{dl};12-16 copies of the transgene) (G1L-G93A mice)(Jackson Laboratory, Bar Harbor, ME, USA). The amount of human SOD1 in RBC lysates of G1H-G93A mice was 3.4 times higher than the G1L-G93A mice (Gurney et al., 1994). The G93A rat was a transgenic line (G93A-39) in which the level of human SOD1 with the G93A mutation was 2.5 times the level of endogenous rat SOD1 (Nagai et al., 2001). The H46R rat used in this study was a transgenic line (H46R-4) in which the level of human SOD1 with the H46R mutation was 6 times the level of endogenous rat SOD1 (Nagai et al., 2001).

The G1H-G93A mice were examined the liver and the spinal cord specimens at 90 (n=2), 100 (n=2), 110 (n=3) and 120 (n=3) days of age. The G1L-G93A mice were examined at 90 (n=1), 100 (n=1), 120 (n=1), 150 (n=1), 180 (n=1), 190 (n=1), 215 (n=1), 230 (n=1) and over 250 (n=2) days of age. As mouse controls, we also examined the liver and the spinal cord specimens of each of ten age-matched littermates of the G1H-G93A and G1L-G93A mice. The G93A rats were examined at 70 (n=1), 90 (n=1), 110 (n=1), 130 (n=1), 150 (n=1) and over 180 (n=3) days after birth. The H46R rats were sacrificed for spinal cords at 110 (n=1), 135 (n=1), 160 (n=1), 170 (n=2) and over 180 (n=3) days after birth and were examined for livers at over 180 days after birth. The detailed clinical signs and pathological characteristics of the H46R and G93A rats have been demonstrated previously (Nagai et al., 2001). As rat controls, we investigated the spinal cord specimens of each of eight age-matched littermates of H46R and G93A rats. Mice and rats were anesthetized with sodium pentobarbital (0.1 ml/100g body weight). After perfusion

of the animals via the aorta with physiological saline at 37°C, they were fixed by perfusion with 4% paraformaldehyde in 0.1 M cacodylate buffer (pH 7.3). The livers and the spinal cords were removed and then postfixed in the same solution. This study was approved by the Institutional Animal Care and Use Committee of Tottori University (Permission No. 03-S-18).

Autopsy specimens

Histochemical and immunohistochemical studies were performed on archival, buffered 10% formalin-fixed, paraffin-embedded liver and spinal cord tissues obtained at autopsy from one long-term surviving FALS patient with a clinical course of 11 years. The clinicopathological characteristics of the FALS patient were reported previously (Kato et al., 1996, 1997). SOD1 analysis revealed FALS patient had a two-base-pair deletion at codon 126 (frame-shift 126 mutation) (Kato et al., 1996). As human controls, we examined autopsy specimens of the pathologically normal livers and spinal cord from 5 neurologically and neuropathologically normal individuals (3 male, 2 females; aged 45-68 years).

Histochemistry and immunohistochemistry

After fixation, the specimens were embedded in paraffin, cut into 4-μm-thick or 6-μm-thick sections and examined by light microscopy. Liver sections were stained by hematoxylin and eosin (HE), and spinal cord sections were stained by the following histochemical methods: HE, Klüver-Barrera, Holzer and Bielschowsky stains. Rat PrxI was over-expressed using the *Escherichia coli* strain BL21 (DE3) cells harboring the expression plasmid pET3c (Novagen, Darmstadt, Germany)-PrxI and purified by the methods described previously (Hirotsu et al., 1999a). Rat PrxII, which contained a 6-His-tagged sequence at the amino-terminal region, was over-expressed using the *Escherichia coli* strain BL21 (DE3) cells harboring the expression plasmid pET30a (Novagen, Darmstadt, Germany)-PrxII. The His-tagged PrxII was purified by a Ni^{2+}-nitrilotriacetate column (Qiagen GmhH, Hilden, Germany) and then digested with enterokinase. Finally, the purified PrxII was passed through an Erapture Agarose column for removal of enterokinase (Novagen). The PrxI /PrxII genes were prepared from a rat liver cDNA library (Takara Biomedicals, Otsu, Japan) by PCR using the primers 5'- AGCCATATGTCTTC AGGAAATGCAA -3', forward and 5- TCGGATCC TCACTTCTGCT TAGAGAAA TACTC-3', reverse for PrxI, as well as the primers 5'-TTCCATGGCCTCCG GCAACGCGCACAT-3', forward and the primers 5'-TTGGATCCATCTCAGTTGTGTTTGGAG-3', reverse for PrxII, respectively. NdeI/BamHI and NcoI/BamHI sites were underlined. Utilizing these purified recombinant rat PrxI (amino acids 1–199) and PrxII (amino acids 1–198), the rabbit polyclonal antibodies against the recombinant rat PrxI/PrxII were prepared by the modified method of Kato et al. (2004).

Representative paraffin sections were used for immunohistochemical assays. The following primary antibodies were used: a newly-produced rabbit polyclonal antibody against rat PrxI [diluted 1:2000 in 1% bovine serum albumin-containing phosphate-buffered saline (BSA-PBS), pH 7.4], a newly-produced rabbit polyclonal antibody against rat PrxII [diluted 1: 2,000 in 1% BSA-PBS, pH 7.4], an affinity–purified rabbit antibody against a synthetic peptide corresponding to the carboxyl terminal region of PrxII (amino acids 184-198: NH2-KPNVDDSKEYFSKHN-COOH. These amino acid sequences are homologous with those of each carboxyl terminal region of the human, rat or mouse PrxII.) (concentration: 1 μg/ml) (Kato et al., 2004), a polyclonal antibody to GPxI [diluted 1: 2,000 in 1% BSA-PBS, pH 7.4] (Kato et al., 2004).

Anti-PrxI antibody was applied to liver sections and anti-PrxII antibody was applied to spinal cord and liver sections because PrxI was contained in the liver but was not contained in the neuron and PrxII was localized in both the neuron and the liver. Sections were deparaffinized, and endogenous peroxidase activity was quenched by incubation for 30 min with 0.3% H_2O_2. The sections were then washed in PBS. Normal serum homologous with the secondary antibody was used as a blocking reagent. Tissue sections were incubated with the primary antibodies for 18 h at 4°C. PBS-exposed sections served as controls. With respect to the preabsorption test, some sections were incubated with anti-PrxI or anti-PrxII polyclonal antibody that had been preabsorbed with an excess amount of the PrxI or PrxII peptide, respectively. Bound antibodies were visualized by the avidin-biotin-immunoperoxidase complex (ABC) method using the appropriate Vectastain ABC Kit (Vector Laboratories, Burlingame, CA, USA) and 3,3'-diaminobenzidine tetrahydrochloride (DAB; Dako, Glostrup, Denmark) as chromogen.

Western blot analysis

This analysis was carried out on 20 fresh specimens from the livers of G1H-G93A mice at 4 different points after birth: 90 days of age (n=2), 100 days of age (n=2), 110 days of age (n=3), and 120 days (n=3). Specimens of livers from control littermate mice were also taken at 4 different points after birth: 90 days of age (n=2), 100 days of age (n=2), 110 days of age (n=3), and 120 days (n=3). In brief, specimens were homogenized in Laemmli sample buffer (Bio-Rad, Hercules, CA, USA) containing 2% sodium dodecyl sulfate (SDS), 25% glycerol, 10% 2-mercaptoethanol, 0.01% bromophenol blue, and 62.5 mM Tris-HCl (pH 6.8). The samples were heated at 100°C for 5 min. Exact 20-μg amounts of soluble protein extracts from the samples were separated on SDS-polyacrylamide gels (4%-20% gradient, Bio-Rad) and transferred by electroblotting to Immobilon PVDF (Milipore, Bedford, MA, USA). After blocking

with 5% nonfat milk for 30 min at room temperature, the blots were incubated overnight at 4°C with the antibody against PrxI. Binding to PrxI was visualized with the Vectastain ABC Kit and DAB. Appropriate molecular weight markers (Bio-Rad) were included in each run.

Results

Clinical course and histopathology

G1H-G93A transgenic mice

The time of clinical onset in the G1H-G93A mice was approximately 100 days after birth. The number of anterior horn cells in the spinal cord of the G1H-G93A mice examined at 90 days after birth was not significantly lower than that of the age-matched littermates, whereas neuropil vacuolation was observed. The anterior horn cells in the G1H-G93A mice at 100 days of age were slightly less abundant and contained many vacuoles and a few Lewy body-like hyaline inclusions (LBHIs). The G1H-G93A mice examined at 110 and 120 days of age revealed severe loss of the anterior horn cells, and also showed many inclusions and neuropil vacuoles, i. e., they had inclusion- and vacuolation-pathologies. The spinal cords of the littermate mice did not show any distinct histopathological findings.

In the presymptomatic stage of the first 90 days after birth, two kinds of cells- swollen hydropic hepatocytes and eosinophilic hepatocytes-were found (Fig. 2A). The swollen hepatocytes had clear nuclei and a bright half-translucent cytoplasm that contained a few vacuoles about 5 μm in diameter. The eosinophilic hepatocytes had condensed nuclei and a dark eosinophilic cytoplasm with some vacuoles about 2 μm in diameter. The population of swollen hepatocytes was about 70% of total hepatocytes and the eosinophilic cells accounted for the remainder (Table 1). The eosinophilic hepatocytes were scattered and intermingled among the swollen hepatocytes. Some intersinusoidal cells also contained vacuoles about 1 μm in diameter. Although both kinds of hepatocytes were still observed at 100 days of age, the small sized-eosinophilic hepatocytes represented about 80% of the cell population and the proportion of swollen hepatocytes was correspondingly lower (Fig. 2B). Fewer

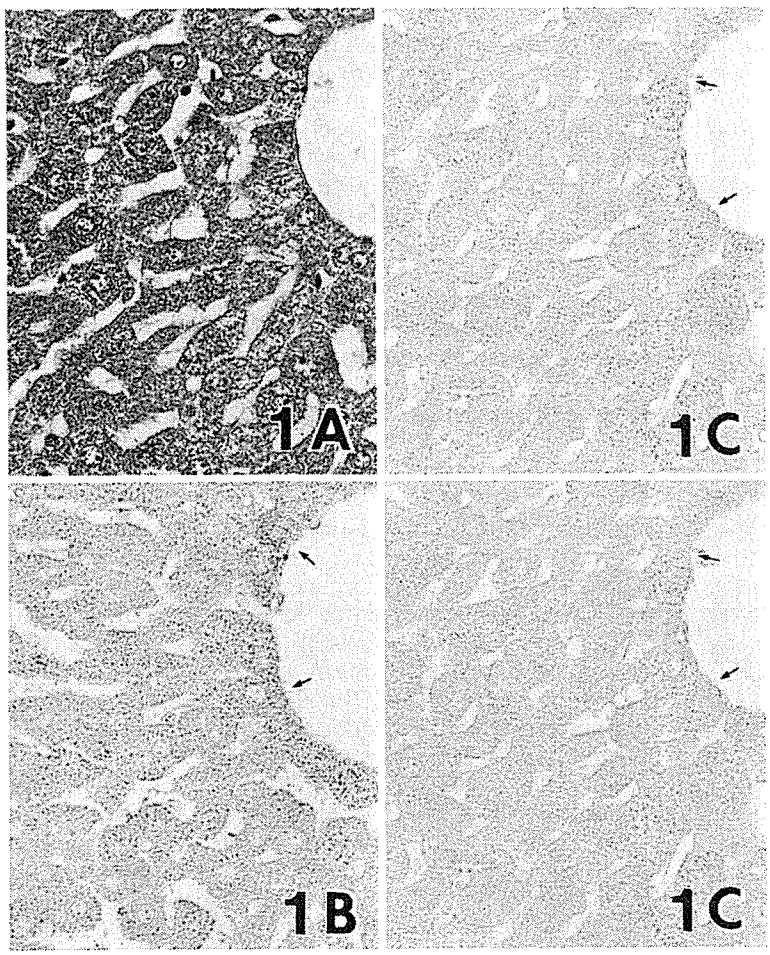

Fig. 1. Hematoxylin and eosin (HE) staining **(A)**, and immunohistochemical staining of the liver sections in control littermate mice for Peroxiredoxinl (Prxl) **(B)**, Peroxiredoxinll (Prxll) **(C)** and Glutathione peroxidasel (GPxl) **(D)**. **A.** The livers of the littermate mice do not show any distinct histopathological findings. **B-D.** Prxl, Prxll and GPxl are expressed in the cytoplasm of almost all hepatocytes. Hepatocytes in the periportal areas stain more strongly for Prxl/Prxll/GPxl than those in the periterminal vein areas (arrows). x 230

vacuoles were present in the cytoplasm of the swollen hepatocytes, although the size of the vacuoles was unchanged. The vacuoles of the eosinophilic hepatocytes became smaller than those of the eosinophilic hepatocytes at 90 days of age, (~1 μm in diameter). Most intersinusoidal cells had shrunken cytoplasm with small (~1 μm) vacuoles. At 110 days of age, almost all of the hepatocytes were normal in HE preparations; neither swollen hydropic hepatocytes nor eosinophilic hepatocytes were observed. No vacuoles were observed in the hepatocytes or intersinusoidal cells. The histological findings in the liver at 120 days of age, corresponding to the end stage (Fig. 2C), were almost the same as those of the control G1H-G93A littermate mice. The intersinusoidal cells also appeared normal in HE preparations. In contrast to the anterior horn cells in the spinal cord, intracytoplasmic eosinophilic inclusions like LBHIs were not observed in the hepatocytes throughout the disease course. The livers of the G1H-G93A littermate mice did not show any distinct histopathological findings (Fig. 1A). Dramatic histopathological changes in the G1H-G93A mouse hepatocytes were observed during the disease course from the presymptomatic stage to the onset (Table 1), in marked contrast to the situation in the spinal cord.

G93A and H46R transgenic rats

The clinical courses and neuropathological findings in G93A and H46R transgenic rats have been reported by Nagai et al. (2001). As expected, the G93A rats showed clinical motor signs at around 125 days of age, and the G46R rats developed motor deficits at approximately 145 days of age. When we focused on the anterior horn cells of the spinal cords of G93A rats, the numbers of anterior horn cells at 70, 90 and 110 days of

Table 1. Histopathological characteristics in the livers of G1H-G93A and G1L-G93A mice and G93A rats during the course of the disease.

G1H-G93A mice	Presymptomatic stage					The onset		Motor deficit stage	End stage
Days after birth	90 days					100 days		110 days	120 days
HE staining	Swollen hepatocytes		Eosinophilic hepatocytes			Swollen hepatocytes	Eosinophilic hepatocytes	Normal hepatocytes	Normal hepatocytes
Percentage*	76 ± 2%		24 ± 2%			17 ± 3%	83 ± 3%	100%	100%
Size of vacuoles	5 μm		2 μm			5 μm	1 μm	-	-
G93A rat	**Presymptomatic stage**					**The onset**		**Motor deficit stage**	**End stage**
Days after birth	70 days	90 days	110 days			130 days		150 days	Over 180 days
HE staining	Normal hepatocytes	Normal hepatocytes	Swollen hepatocytes	Eosinophilic hepatocytes	Normal hepatocytes	Small-sized hepatocytes		Small-sized hepatocytes	Normal hepatocytes
Percentage*	100%	100%	83 ± 1%	3%	14 ± 1%	100%		100%	100%
Size of vacuoles	-	2 μm	3 μm	1 μm	-	1 μm		1 μm	-
G1L-G93A mice	**Presymptomatic stage**					**The onset**		**Motor deficit stage**	**End stage**
Days after birth	110 days	120 days	150 days			180 days	190 days	215 days	Over 250 days
HE staining	Normal hepatocytes	Normal hepatocytes	Swollen hepatocytes		Normal hepatocytes	Swollen hepatocytes	Swollen hepatocytes	Small-sized hepatocytes	Normal hepatocytes
Percentage*	100%	100%	73 ± 5%		27 ± 5%	100%	100%	100%	100%
Size of vacuoles	1~2 μm	2 μm	5 μm		2 μm	5 μm	5 μm	2 μm	-

Percentage* means the percentage of each hepatocyte number to total cell number.

age were almost the same as for the age-matched littermates of G93A rats, although the G93A rats at 90 and 110 days of age showed vacuolation-pathology including neuropil vacuoles. At 70 days of age, no distinct histological changes were found in the livers of the G93A rats. At 90 days of age, a few vacuoles of about 2 μm in diameter began to appear in the cytoplasm of the normal appearing hepatocytes (Table 1). The intersinusoidal cells appeared almost normal. At 110 days of age, in the preclinical stage, swollen hydropic

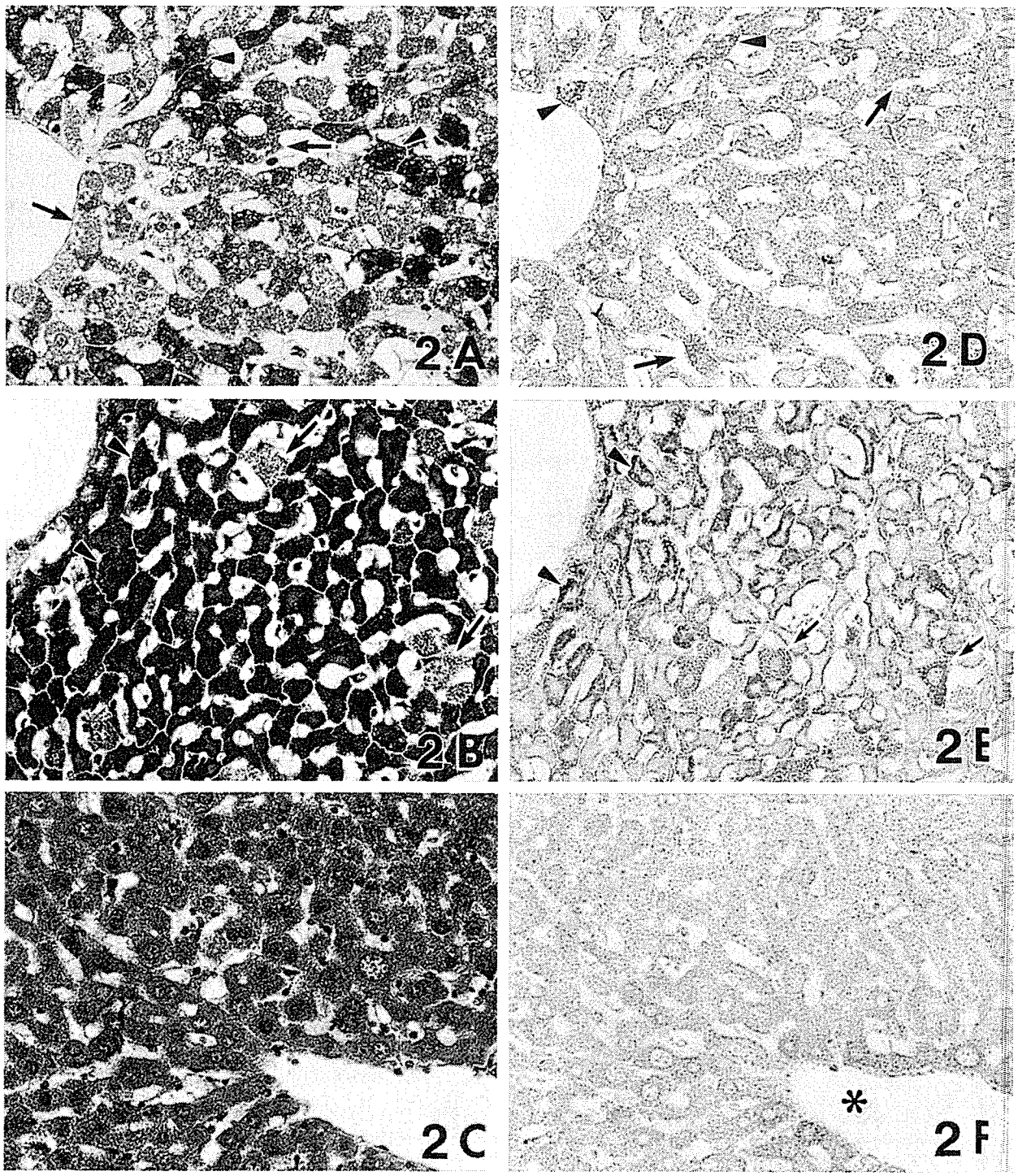

hepatocytes and dark eosinophilic hepatocytes were observed in addition to normal hepatocytes. These two types of hepatocytes in G93A rats were histologically identical to those in HE preparations from G1H-G93A mice. The proportions of each type of hepatocytes were: swollen hydropic hepatocytes, approximately 83%,; eosinophilic hepatocytes, about 3%,; normal hepatocytes, about 14%. The swollen hepatocytes contained some vacuoles about 3 μm in diameter. The eosinophilic hepatocytes shrunken and the dense eosinophilic cytoplasm contained vacuoles about 1μm in diameter. However, the normal appearing hepatocytes at 110 days of age did not contain vacuoles. The intersinusoidal cells contained small (~1 μm) vacuoles. In G93A rats at 130, 150 and over 180 days of age, there was a loss of anterior horn cells in association with both inclusion- and vacuolation-pathologies. In marked contrast, almost all of the hepatocytes appeared histologically normal in HE preparations and were smaller than those of the littermates. Some hepatocytes at 130 days of age contained vacuoles about 1 μm in diameter (Fig. 3A). Beyond 180 days of age, the period corresponding to the end stage when there were marked losses of anterior horn cells, most hepatocytes of both G93A and H46R rats were normal in HE preparations, although a few small vacuoles were observed in some hepatocytes (Table 1). The intersinusoidal cells also appeared almost normal.

G1L-G93A transgenic mice

As expected, the time of clinical onset in the G1L-G93A mice from Jackson Laboratory was approximately 185 days after birth. In the G1L-G93A mice examined at 90, 100, 120, 150 and 180 days after birth, the number of anterior horn cells was not significantly changed in contrast with that of the age-matched littermates of G1L-G93A mice, although the G1L-G93A mice at 90, 100, 120, 150 and 180 days of age showed vacuolation-pathology and the G1L-G93A mouse at 180 days of age showed a few inclusions. In G1L-G93A mice at 190, 215, 230 and over 250 days of age, there were significant losses of anterior horn cells, and both inclusion- and vacuolation-pathologies were present.

At the preclinical stage of 110 and 120 days of age, vacuoles about 2 μm in diameter were already present in the cytoplasm of the hepatocytes in the G1L-G93A mice, although the structures of hepatic lobules and hepatocytes appeared normal (Table 1). At 150,180 and 190 days of age, many hepatocytes showed hydropic change: approximately 60% of hepatocytes at 150 days of age were swollen hepatocytes with hydropic change, and almost all of the hepatocytes at 180 and 190 days of age were hydropic hepatocytes (Table 1). However, eosinophilic hepatocytes were not conspicuous. In addition, several irregular cytoplasmic slits containing some fluid-like material were outstanding in the hepatic cytoplasm at 180 and 190 days of age (Fig. 3B). At 215 days of age, small hepatocytes were observed, as was the case for the G93A rats at 150 days of age. In addition, there were small vacuoles about 2 μm that were distributed in the periphery of the cytoplasm of these small hepatocytes. Beyond 250 days of age, the period corresponding to the end stage, the hepatocytes appeared almost normal in HE preparations. The intersinusoidal cells were almost normal after 215 days of age although some vacuoles were seen in the cytoplasm from 110 days to 190 days of age.

A long-term surviving FALS patient with a frame-shift 126 mutation in the SOD1 gene

The clinical course and histopathological findings of this FALS patient with a clinical course of 11 years were reported previously by Kato et al. (1996). Severe neuronal loss with gliosis was recognized in the anterior

Fig. 2. A-C. Hematoxylin and eosin (HE) staining of liver sections of G1H-G93A transgenic mice in the pre-symptomatic stage of the first 90 days after birth **(A)**, at the onset of 100 days after birth **(B)** and at the end stage of 120 days after birth **(C)**. **D-F.** Immunohistochemical findings for peroxiredoxinI (PrxI) of liver sections of G1H-G93A mice in the presymptomatic stage of the first 90 days after birth **(D)**, at the onset of 100 days after birth **(E)** and at the end stage of 120 days after birth **(F)**. **A.** In the presymptomatic stage, two kinds of cells of swollen hydropic hepatocytes (arrows) and eosinophilic hepatocytes (arrowheads) are seen. The swollen hepatocytes have clear nuclei and a bright half-translucent cytoplasm that contain a few vacuoles about 5 μm in diameter. The eosinophilic hepatocytes have condensed nuclei and a dark eosinophilic cytoplasm with some vacuoles about 2 μm in diameter. The population of swollen hepatocytes is about 70% of total hepatocytes and the eosinophilic cells account for the remainder. The eosinophilic hepatocytes are scattered and intermingled among the swollen hepatocytes. **B.** At the onset stage, small sized-eosinophilic hepatocytes (arrowheads) represent about 80% of the cell population and the proportion of swollen hepatocytes (arrows) is correspondingly lower. Fewer vacuoles are present in the cytoplasm of the swollen hepatocytes. The vacuoles of the eosinophilic hepatocytes become smaller than those of the eosinophilic hepatocytes at 90 days of age. **C.** At the end stage, almost all of the hepatocytes are normal; neither swollen hydropic hepatocytes nor eosinophilic hepatocytes are observed. No vacuoles are observed in the hepatocytes. The histological findings in the liver at 120 days of age, corresponding to the end stage, are almost the same as those of the control G1H-G93A littermate mice. **D.** PrxI immunostaining of the hepatocytes in the pre-symptomatic stage. The PrxI-negative hepatocytes are intermingled with the positive hepatocytes in the pre-symptomatic stage. The normal zonal distributions of PrxI disappear in the pre-symptomatic stage. Approximately 80% of the swollen hepatocytes (arrows) and about 30% of the eosinophilic hepatocytes observed in HE preparations show immunoreactivity to PrxI. The other hepatocytes are negative for PrxI. Although most of the PrxI-expressing hepatocytes show the same staining intensity as that of control littermate hepatocytes, a few eosinophilic hepatocytes (arrowheads) strongly express PrxI. **E.** PrxI immunostaining of the hepatocytes at the onset. PrxI is overexpressed in both eosinophilic (arrowheads) and swollen hepatocytes (arrows). The staining intensity of the hepatocytes that are positive for PrxI is strongest at this stage. The normal zonal distribution of PrxI is not observed; a few negative hepatocytes are intermixed with the PrxI-positive hepatocytes. **F.** PrxI immunostaining of the hepatocytes at the end stage. Almost all of the hepatocytes show the same stainability and intensity as those of the hepatocytes of the normal littermates. Normal zonal distribution of PrxI is observed in this stage: hepatocytes in periportal areas stain more strongly for PrxI than those in the periterminal vein areas (asterisk). x 240

horn cells of the spinal cord, and neuronal LBHIs and astrocytic hyaline inclusions (Ast-His) were present (Kato et al., 1996, 1997). The liver showed neither fibrosis nor inflammation (Fig. 4A). Although no inclusion pathology such as neuronal LBHIs and Ast-His was evident in the hepatocytes, vacuolation pathology was obsereved in the hepatocytes (Fig. 4A).

Immunohistochemistry

Immunohistochemical findings in spinal cords of transgenic animals

When control and representative paraffin sections were incubated with PBS alone (i.e., no primary antibody), no staining was detected. The neuronal Lewy body-like hyaline inclusions (LBHIs) in ALS model animals with human mutant SOD1exhibited co-aggregation of PrxII/GPxI with SOD1. A breakdown of the redox system was observed in these motor neurons, which formed inclusions due to co-aggregation of PrxII/GPxI with SOD1. The PrxII/GPxI-immunoreactions in the four different phyletic lines of the ALS rat models (H46R and G93A rats) and ALS mouse models (G1H-G93A and G1L-G93A mice) were essentially the same throughout the disease course. In the preclinical stage, the PrxII/GPxI-immunostainability and immunointensity of the anterior horn cells were identical to those in normal anterior horn cells in the littermates. Although anterior horn cells in the ALS

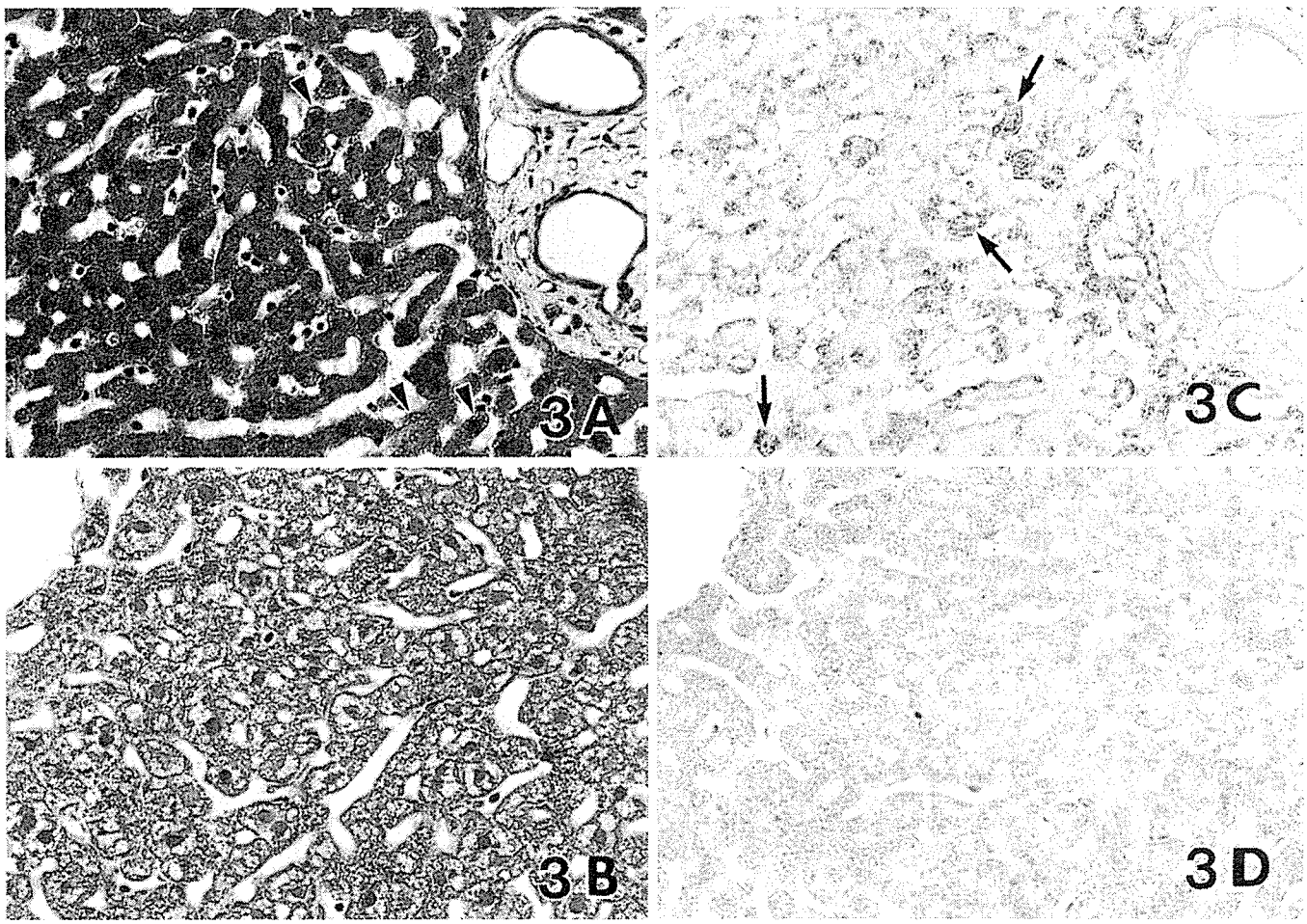

Fig. 3. A,B. Hematoxylin and eosin (HE) staining of the liver sections of G93A transgenic rats in the time of clinical onset at the age of 130 days after birth and of G1L-G93A transgenic mice in the presymtomatic stage at the age of 180 days after birth. **C, D.** Immunohistochemical staining of peroxiredoxinI (PrxI) in the liver sections of G93A transgenic rats in the time of clinical onset at the age of 130 days after birth and of G1H-G93A transgenic mice in the presymtomatic stage at the age of 180 days after birth. **A.** In G93A rats at 130 days of age, almost all of the hepatocytes appear histologically normal and are smaller than those of littermates. Some hepatocytes at 130 days of age contain about 1 μm in diameter (arrowheads). **B.** In G1L-G93A mice at 180 days of age, almost all of the hepatocytes are hydropic. In addition, several irregular intracytoplasmic slits containing some fluid-like material are seen. **C.** At 130 days of age in G93A rats, small hepatocytes that are predominant in HE preparations expressed PrxI intensely (arrows). **D.** At 180 days of age in G1L-G93A mice, the hepatocytes are immunostained intensely with the antibody against PrxI and the intracytoplasmic slits in hepatocytes are also strongly positive for PrxI. x 240

animal models were less abundant after clinical onset, some of these residual anterior horn cells overexpressed Prxll/GPxl, i.e., there was upregulation of the redox system. This upregulation in the residual motor neurons was most pronounced at 110 days of age in G1H-G93A mice, at 150 days in G93A rat, at 215 days in G1L-G93A mouse, and at 160 days in H46R rat. However, at the end stage in the four different strains of ALS model animals, almost all of the residual motor neurons showed no immunoreactivity for Prxll/GPxl, that is, they had undergone redox system breakdown, in marked contrast to the inclusions, which were positive for PrxII/GPxI.

Immunohistochemical findings in G1H-G93A transgenic mouse livers

In control littermate mice, PrxI, PrxII and GPxI (PrxI/PrxII/GPxI), which directly regulate the redox system, were expressed in the cytoplasm of almost all hepatocytes (Fig. 1B-D). The nuclei of some hepatocytes were also positive for PrxI and PrxII. Hepatocytes in the periportal areas stained more strongly for PrxI/PrxII/GPxI than those in the periterminal vein areas. Incubation of sections with the anti-rat PrxI or PrxII antibody that had been respectively pretreated with an excess amount of rat PrxI or PrxII produced no staining in any of the sections. The immunohistochemical results are summarized in Table 2. In contrast to the normal hepatocytes that were positive for the three proteins, the PrxI/PrxII/GPxI-negative hepatocytes were intermingled with the positive hepatocytes in the presymptomatic stage at 90 days after birth (Fig. 2D). Therefore, the normal zonal distribution of PrxI/PrxII/GPxI disappeared in the presymptomatic stage. Approximately 80% of the swollen hepatocytes and about 30% of the eosinophilic hepatocytes observed in HE preparations showed immunoreactivity to the redox-related proteins (Table 2). The other hepatocytes were negative for the three proteins. The staining intensity of PrxI/PrxII/GPxI was the same as that of

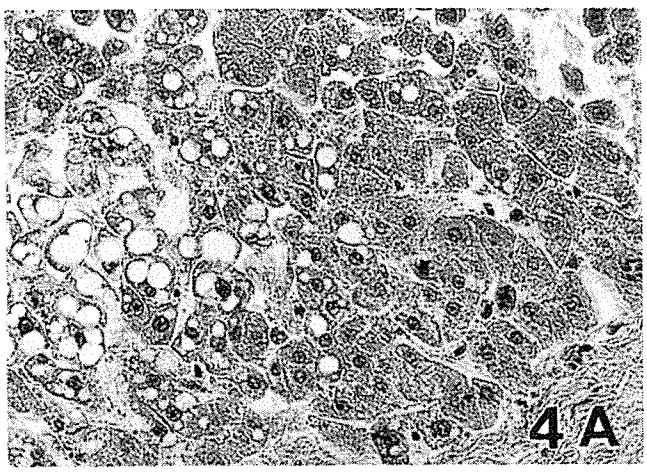

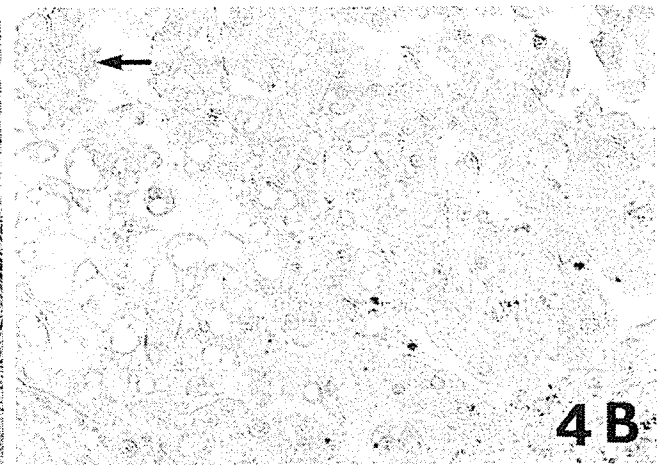

Fig 4. Hematoxylin and eosin staining **(A)** and immunohistohcemical staining of peroxiredoxinl (Prxl) **(B)** of the liver sections of the long-term surviving familial amyotrophic lateral sclerosis patient with a two-base-pair deletion at codon 126 in SOD1 gene. **A.** There are no fibrosis or inflammation in the liver. Although the inclusion pathology in the hepatocytes is not recognized, some vacuoles are observed in some hepatocytes. **B.** Most hepatocytes are faintly stained or unstained with the anti-Prxl antibody although a few hepatocytes weakly express Prxl (arrow). x 240

Fig. 5. Western blot analysis using the antibody against peroxiredoxinl (Prxl) of the liver. An exact 20-μg amount of the soluble protein extract from each sample was applied to each lane. Lane a: Control littermate mouse liver at 90 days after birth, lane b: G1H-G93A transgenic mouse liver at 90 days after birth, lane c: control littermate mouse liver at 100 days after birth, lane d: G1H-G93A transgenic mouse liver at 100 days after birth, lane e: control littermate mouse liver at 110 days after birth, lane f: G1H-G93A transgenic mouse liver at 110 days after birth, lane g: control littermate mouse liver at 120 days after birth, lane h: G1H-G93A transgenic mouse liver at 120 days after birth. A single band at the position corresponding to Prxl (a molecular mass approximately 23 kDa) (arrowhead) is observed in transgenic mice and control littermate mice. The intensity of Prxl immunoreactivity in the G1H-G93A mice at 90 days of age is slightly less than those in the G1H–G93A mice at 110 and 120 days of age whose Prxl immunoreactivity appears to be almost identical to that in the littermate mice. The intensity of Prxl immunoreactivity in the G1H-G93A mice at 100 days of age is slightly stronger than those in the G1H–G93A mice at 110 and 120 days of age. This observation supports the results of Prxl immunohistochemistry.

control littermate hepatocytes. Most hepatocytes expressed these three proteins synchronously. However, certain hepatocytes that were positive for PrxI/PrxII were negative for GPxI, and some hepatocytes negative for PrxI/PrxII were positive for GPxI. At 100 days of age, the normal zonal distribution of PrxI/PrxII/GPxI was not observed; the PrxI/PrxII/GPxI-negative hepatocytes were intermixed with the positive hepatocytes (Fig. 2E). Approximately 75% of the swollen hepatocytes and about 80% of eosinophilic hepatocytes were positive for PrxI/PrxII/GPxI (Table 2). The staining intensity of the hepatocytes that were positive for the three redox-related proteins was strongest at this stage. After the onset and until the end stage, i.e., during the motor deficit stage, almost all of the hepatocytes showed normal stainability with normal intensity: the stainability and intensity in the hepatocytes of the motor deficit stage were identical to those in the littermates' hepatocytes (Fig. 2F). Furthermore, the normal zonal distribution of PrxI/PrxII/GPxI was observed during the motor deficit stage. The expression of PrxI/PrxII/GPxI in the intersinusoidal cells was similar to that of hepatocytes throughout the disease course. Although all intersinusidal cells expressed these three proteins in the liver of G1H-G93A littermates, some intersinusoidal cells were negative in the presymptpmatic stage. Finally, the three redox-related proteins were expressed in the intersinusoidal cells at the end stage.

Immunohistochemical findings in G93A and H46R transgenic rat livers

In control littermate rats, almost all of the hepatocytes expressed PrxI/PrxII/GPxI identically to those in the littermate mouse livers. At 70 and 90 days of age in G93A rats, PrxI/PrxII/GPxI was expressed in the cytoplasm of the hepatoctyes and the zonal distribution was normal. In the presymptomatic stage at 110 days of age in G93A rats, many of both the swollen and eosinophilic hepatocytes were positive for these redox-related proteins, with normal intensity. However, some negative hepatocytes were intermingled with positive hepatocytes. At 130 days of age in G93A rats, small hepatocytes that were predominant in HE preparations expressed these redox-related proteins intensely: the staining intensity was strongest at this stage throughout the disease course (Fig. 3C). At the end stage in G93A and H46R rats, almost all of the hepatocytes showed the same stainability and intensity as those of the hepatocytes of the normal littermates.

Immunohistochemical findings in G1L-G93A transgenic mice liver

In the preclinical stage at 110,120 and 150 days of age, almost all of the normal hepatocytes in HE preparations expressed Prxl/Prxll/GPxl. At 150 days of age, some of the hydropic hepatocytes were moderately positive for Prxl/Prxll/GPxl and other swelling hepatocytes were negative; the negative hepatocytes were intermixed with positive cells. The vacuoles in the cytoplasm of the hepatocytes were almost negative for Prxl/Prxll/GPxl. Prxl/Prxll/GPxl was expressed in some intersinusoidal cells. At 180 and 190 days of age, the hepatocytes were immunostained intensely with the three antibodies against Prxl/Prxll/GPxl and the intracytoplasmic slits in hepatocytes that contained some fluid were also strongly positive for Prxl/Prxll/GPxl (Fig. 3D). At 215 days of age, almost all of the hepatocytes expressed Prxl/Prxll/GPxl. At the end stage, beyond 250 days of age, the stainability and intensity in many hepatocytes were lower than in the hepatocytes in the control littermates, although some hepatocytes showed the same stainability and intensity of Prxl/Prxll/GPxl as those in the control littermates. The intersinusoidal cells showed similar staining patterns to those of hepatocytes.

Immunohistochemical findings in the liver and spinal cord of a long-term surviving FALS patient with a frame-shift 126 mutation in the SOD1 gene

As expected, some neuronal inclusions were positive for PrxII and GPxI in this long-surviving patient. The cytoplasm of the other remaining motor neurons did not express PrxII/GPxI. In the liver, most hepatocytes are faintly stained or unstained with the antibodies against

Table 2. Immunohistochemical results of PrxI/PrxII/GPxI expression in the hepatocytes of G1H-G93A mice .

Days after birth	90 days		100 days		110 days	120 days
Cell type in HE staining	Swollen hepatocytes	Eosinophilic hepatocytes	Swollen hepatocytes	Eosinophilic hepatocytes	Normal hepatocytes	Normal hepatocytes
A ratio of PrxI-positive each-type hepatocytes to each type hepatocytes (PrxI+/each-type total cells)	76.1±2.1%*	32.3±2.0%	78.5±2.5%	40.2±1.8%	100%	100%
PrxII+/each-type total cells	73.8±1.6%	31.4±1.1%	75.5±1.7%	42.0±1.7%	100%	100%
GPxI+/each type total cells	77.0±1.2%	35.1±1.6%	81.1±2.3%	42.1±1.4%	100%	100%

*The number present mean ± standard error.

PrxI/PrxII/GPxI although a few hepatocytes weakly express PrxI (Fig. 4B) /PrxII/GPxI.

Western blot analyses

When homogenates of fresh liver of the G1H–G93A mice were examined by immunoblotting for Prxl, a single band at the position corresponding to a molecular mass of approximately 23 kDa was observed (Fig. 5). Immunoblotting showed that the intensity of Prxl immunoreactivity in the G1H-G93A mice at 90 days of age is slightly less than those in the G1H-G93A mice at 110 and 120 days of age whose Prxl immunoreactivity appears to be almost identical to that in the littermate mice. The intensity of Prxl immunoreactivity in the G1H-G93A mice at 100 days of age is slightly stronger than those in the G1H-G93A mice at 110 and 120 days of age. This observation supported the results of Prxl immunohistochemistry.

Discussion

Although the neuropathology of the motor neurons in ALS including the SALS patients of unknown etiology, mutant SOD1-linked FALS and ALS model animals expressing human mutant SOD1 genes has been investigated in detail (Dal Canto and Gurney, 1995; Wong et al., 1995; Hirano, 1996; Kato et al., 1999), the pathology of the liver has been neglected because failure of liver function is not a feature of ALS. In the present study, for the first time, significant histopathological findings in common were found in both motor neurons and hepatocytes in the four different strains of mutant SOD1-linked ALS model animals. Furthermore, the hepatic histopathological findings changed dramatically during the course of the diseases. The common histopathological findings in the livers in the mutant SOD1-linked ALS model animals were hydropic swelling and eosinophilic changes with vacuolation pathology. Notably, these histopathological changes in the hepatocytes disappeared at the end stage and almost all of the hepatocytes appeared to be normal, not only in HE preparations but also in redox system-related immunohistochemical preparations. Previous histopathological liver findings among SALS patients of unknown etiology included, ultrastructural analyses of liver biopsy findings of 21 ALS patients that showed bizarre mitochondria, intramitochondrial paracrystalline inclusions, disorganization of the lamellar structure of the rough endoplasmic reticulum, more abundant smooth endoplasmic reticulum and parasinusoidal fibrosis (Nakano et al., 1987), but the relationship between these hepatic findings and ALS pathogenesis remains unclear. The present paper is the first to demonstrate significant histopathological findings in hepatocytes during the course of the disease in ALS model animals with a SOD1 mutation as the known etiology.

The common histopathological findings in the livers of the four different phyletic lines of the ALS rat models (H46R and G93A rats) and ALS mouse models (G1H-G93A and G1L-G93A mice) were hydropic swelling and eosinophilic changes with vacuole formation though there were some differences in the copy number of the transgene. The first prominent histopathological finding in the livers of G1H-G93A mice was hydropic degeneration or ballooned swelling of hepatocytes before and around the onset of neurological symptoms. The second striking finding was cytoplasmic eosinophilic degeneration with nuclear condensation of hepatocytes around the time of onset. These two main findings were similar to ballooning or atrophic changes in hepatocytes in acute intoxication after administration of chemical substances such as carbon tetrachloride (Yeldandi et al., 1996). These histopathological findings seem to coincide with hepatic degeneration in drug-induced hepatic injury (Yeldandi et al., 1996). Therefore, it was suggested that the histopathological features of the G1H-G93A liver reflect a type of intoxication by human mutant SOD1 protein that originates from the human SOD1 gene with the G93A mutation.

Vacuolation pathology and motor neuron death with inclusion pathology in the spinal cord are the essential neuropathological findings in ALS model animals (Dal Canto and Gurney, 1995; Wong et al., 1995; Kato et al., 1999). The vacuolation pathology was found before onset of the neurological symptoms (Dal Canto and Gurney, 1995; Wong et al., 1995). Similar vacuole formation was found in the hepatocytes before the onset of neurological symptoms, as it was in motor neurons. From the fact that the vacuolation pathology was observed in both motor neurons and hepatocytes at almost the same disease stage, the common ALS stress of mutant SOD1 is considered to cause histopathological changes of the liver and the spinal cord of ALS model animals in the early stage of the disease. The comparison between hepatocytes and motor neurons is meaningful from the viewpoint of generalized mutant SOD1 disease. Although the hepatocytes and motor neurons in the ALS model animals were under the same ALS stress in the early stages, the histopathological features of the hepatocytes were different from those in motor neurons at the end stage. In other words, the number of motor neurons fell gradually and the inclusion pathology appeared toward the end stage; however, cell death with inclusion pathology was not found in the hepatocytes. We showed that there was a difference in immunohistochemical expression of the redox system related proteins PrxI, PrxII and GPxI to explain this discrepancy between hepatocytes and motor neurons.

The zonal localization of PrxI and GPxI-expressing hepatocytes in the hepatic lobules of the control livers was consistent with previous reports (Sunde and Hoekstra, 1980; Immenschuh, 2003), and this immunohistochemical finding implies that the liver contains abundant redox system-related enzymes. In association with the histopathological changes in the livers from the presymptomatic stages to the onset of neurological symptoms in G1H-G93A mice, the zonal